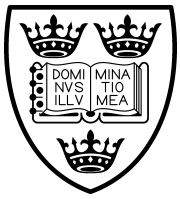
The thinning of the liquid layer over a probe in two-phase flow



James Oliver

St Anne's College

University of Oxford

A thesis submitted for the degree of

Master of Science

September 1998

Acknowledgements

I would like to thank my supervisor Dr Peter Howell for supererogatory help and encouragement over the past four months. I have had numerous helpful discussions with Professor Anthony Pearson, to whom I am very grateful. Many thanks to Dr John Ferguson for presenting the problem and to Chris Breward for his thoughts and help with proof-reading. Also, many thanks to my family and Natasha for their support. Finally, I gratefully acknowledge the E.P.S.R.C. for financial support.

Abstract

The draining of the thin water film that is formed between a two dimensional, infinite, initially flat oil-water interface and a smooth, symmetric probe, as the interface is advected by a steady and uniform flow parallel to the probe axis, is modelled using classical fluid dynamics.

The governing equations are nondimensionalised using values appropriate to the oil extraction industry. The bulk flow is driven by inertia and, in some extremes, surface tension while the viscous effects are initially confined to thin boundary layers on the probe and the interface. The flow in the thin water film is dominated by surface tension, and passes through a series of asymptotic regimes in which inertial forces are gradually overtaken by viscous forces. For each of these regimes, and for those concerning the earlier stages of approach, possible solution strategies are discussed and relevant literature reviewed.

Consideration is given to the drainage mechanism around a probe which protrudes a fixed specified distance into the oil. A lubrication analysis of the thin water film may be matched into a capillary-static solution for the outer geometry using a slender transition region if, and only if, the pressure gradient in the film is negative as it meets the static meniscus. The remarkable result is that, in practice, there is a race between rupture in the transition region and rupture at the tip. The analysis is applicable to the case of a very slow far field flow and offers significant insight into the non-static case.

Finally, a similar approach is applied to study the motion of the thin water film in the fully inviscid approximation, with surface tension and a density contrast between the fluids.

Contents

1 Introduction **1**

1.1 Industrial motivation 1

1.2 Discussion and a model problem 5

1.3 Thesis structure 7

2 Formulation of the problem **8**

2.1 Fundamental assumptions and the governing equations 8

2.2 Nondimensionalisation 10

2.3 The dimensionless parameter groups 11

3 Asymptotic regimes **13**

3.1 Preliminaries 13

3.2 Asymptotic regimes 14

3.2.1 Early stage of approach 14

3.2.2 Initial deformation of the interface 15

3.2.3 The thinning phases 16

3.2.4 Single-phase flows 17

3.3 Summary 23

4 The quasi-static viscous case **24**

4.1 Introduction 24

4.2 Governing equations in the new coordinate system 26

4.2.1 Geometry of the substrate 26

4.2.2 The new coordinate system 26
4.2.3 Governing equations 27
4.3 The outer problem 29
4.3.1 Analytic solution 29
4.3.2 Example: The circular cone tip 31
4.3.3 The outer matching condition 32
4.4 Thin film analysis 33
4.4.1 Preliminaries 34
4.4.2 Driving forces and nondimensionalisation 34
4.4.3 Asymptotic expansions 35
4.4.4 The leading-order problem 35
4.4.5 The evolution equation for the film height 36
4.4.6 Analysis and discussion 37
4.5 Transition region on a curved arc 39
4.6 Conclusions and extensions 44

5 The inertial thinning phase **48**
5.1 Preliminaries 48
5.2 The thin film problem 49
5.3 Summary and extensions 53

6 Conclusions and Future Work **54**
6.1 Summary and discussion 54
6.2 Future work 57

Chapter 1

Introduction

1.1 Industrial motivation

Multiphase flows occur in many diverse fields of science, engineering and industry. Characteristic examples are blood flow, atmospheric precipitation, convection of the Earth's mantle and the brewing of beer. We consider the industrial process of oil extraction where generically, oil droplets and gas bubbles (which hereafter we refer to as *cells*) are suspended in a continuous water phase. The mixture (which may be highly contaminated with naturally occuring pollutants) is pumped through a vertical pipe (with diameter much larger than that of a typical cell) which extends several miles underground to the source. For the purposes of production logging in the field, it is necessary to measure the time-averaged local phase fractions and flow rates at various points in the pipe. One well-known class of techniques is based on the use of small needle-like probes which measure a property of the fluid surrounding their tips.

There are many different types of probe which are distinguished by their material build, surface geometry and the fluid property they measure. However, nearly all are radially symmetric and have a diameter of not more than a few hundred microns; much smaller than the diameter of a typical cell. A probe is aligned with the uniform global water velocity and made small so as to disturb the flow as little as possible. Figure 1.1 shows some typical probe tip geometries.

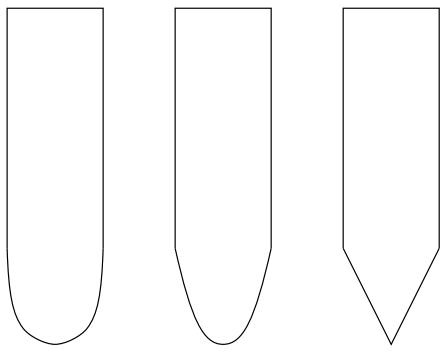


Figure 1.1: Typical cross-sectional geometries of probe tips.

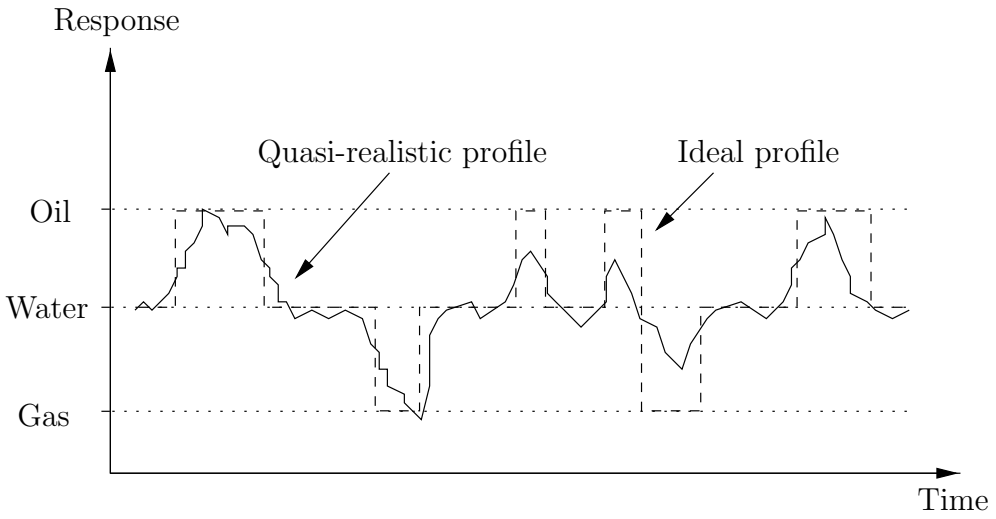


Figure 1.2: Time-series response graphs.

The two most common types of probe are (i) electrical, measuring the conductivity or impedance at the probe tip and (ii) optical, measuring the reflectivity at the end of an optical fibre. Details concerning the engineering and testing of the most widely-used probes may be found in Billingham & King [2].

The usual measurement principle assumes that the probe is so small that the distribution of the phases in the neighbourhood of the probe is exactly what it would be if the probe where not there. This, the simplest assumption that can be made, corresponds to the ideal situation where:

- the cells are not deformed by the probe;
- the interface separating the cells from the continuous phase is instantaneously ruptured by the probe at entry and exit;
- the contact line follows the path of the "undisturbed" interface; see the dotted line in figure 1.3);
- the signal is determined instantaneously by the phase at the tip.

The resulting time-series response graph would therefore consist entirely of square-waves, as in the dashed lines in figure 1.2. In practice a distinctly more irregular pattern is observed; see the solid line in figure 1.2. The rise and fall in the signal is not sharp and does not always reach the "full" height. This is thought to be due to the interaction of the probe measurement mechanism and the three following fluid phenomena.

(i) Grazing, where cells do not hit the probe centrally *and* normally.

(ii) The drainage mechanism, since a cell will not be immediately penetrated upon reaching the probe; see the solid line in figure 1.3.

(iii) The lagging of the 3-phase contact line (which forms on the probe surface upon its penetration of the interface) behind the bulk interface; see the dashed line in figure 1.3.

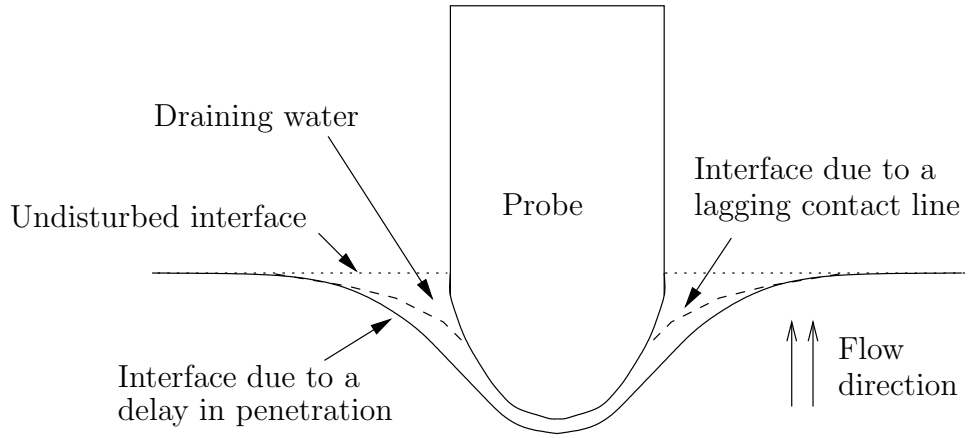


Figure 1.3: Schematic diagram of the possible local configurations of an oil-water interface as the parent oil droplet passes over the probe tip.

The extent to which (ii) and (iii) may affect the signal depends upon the effective size and shape of the *measurement neighbourhood* N surrounding the probe tip, over which the measurement mechanism takes its average. If the interface enters N before it has had time to rupture, we expect (ii) to have a significant effect on the probe signal. Similarly, there is a significant effect if the 3-phase contact line lags behind in N . We propose that there are probes for which one or both of these effects is significant. Indeed, it seems likely that the first will dominate for a rounded probe tip, while the second will dominate for a sharp probe tip, so that there must be an intermediate case in which both are significant. Hereafter, we refer to these two effects as the *drainage delay effect* and the *lagging contact line effect*, respectively.

In the field, the time-series is averaged (using a so-called *phase criterion* to distinguish between the oil, gas and water) to give a local volume fraction of the dispersed phases. Experiment has shown that the final results are not too bad, although the errors are sufficiently large to cause unwanted inaccuracies.

The local time-averaged phase flow rates may also be measured by connecting together two identical probes with their ends slightly out of alignment. Such a device is called a *dual local probe* and Schlumberger Cambridge Research (SCR) are very interested in optimising its performance in the field. The idea is that there is a time delay in response from the leading to the trailing probe as a cell passes over the device (see figure 1.4). In practice the two signals have an irregular profile, as described above, and occasionally a rise or fall is seen in only *one* of them; a phenomenon that can be explained by grazing.

Figure 1.5 contains schematics of ideal and observed time-series response graphs. The signals are cross-correlated (via a *phase criterion*) to obtain the required velocities. Again, the results are acceptable, but the errors are enough to cause problems. The global time-averaged phase fractions and flow rates across a cross-section of the pipe are easily found by taking a number of local measurements and integrating across the flow field. The *ideal assumption*, together with a *phase criterion*, and the ideas introduced above form the backbone of Schlumberger's current interpretation of the dual local probe measurements. Their aim is to improve on this interpretation and find the "best" probe design for use in the field. This means that it must be as cheap as possible to manufacture, yet sufficiently robust and accurate to provide good results over a sustained period. We comment that the flat-ended cylindrical probe is the easiest (and therefore the cheapest) to manufacture. Unfortunately, it gives totally unacceptable results.

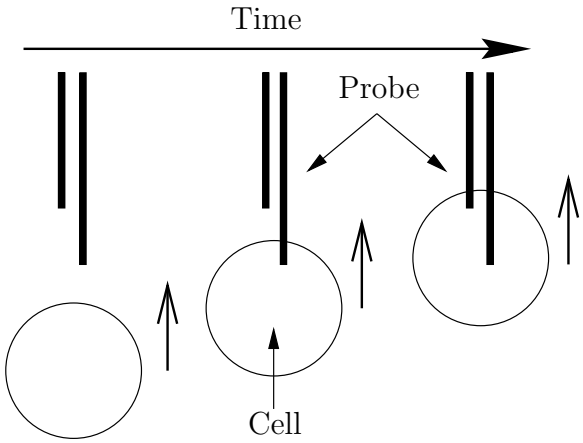


Figure 1.4: Schematic diagram of a dual local probe penetrating an oil droplet. (Not to scale: the cell is much bigger in practice.)

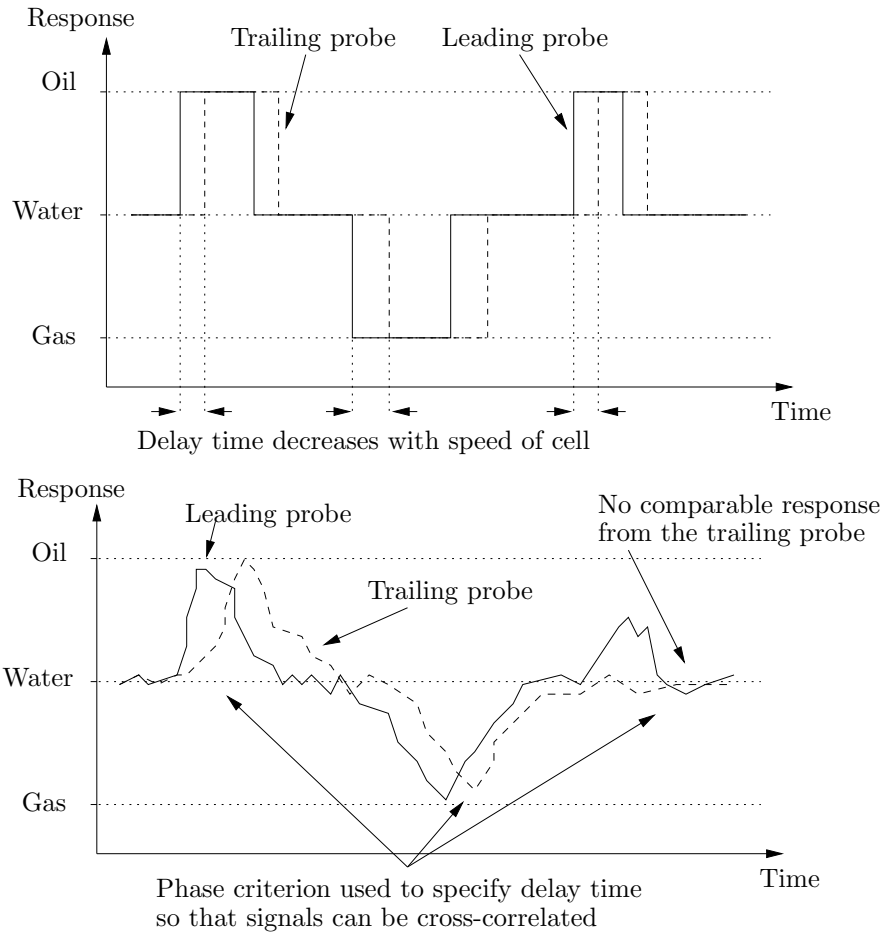


Figure 1.5: Quasi-realistic time-series response graphs for the ideal case (above) and in practice (below).

1.2 Discussion and a model problem

Given a set of initial conditions for an approaching cell, the idealist would like to know the following:

- the interface position and phase flow fields as the cell approaches, drains, ruptures and moves past a local probe, together with how these depend on the fluid and probe properties;
- the resulting output signal from the probe tip as a function of the instantaneous distribution of the flow fields in the measurement neighbourhood N, together with the significance of the drainage delay and lagging contact line effects.

The flow problem is inherently very difficult because of the presence of free boundaries and 3-phase contact lines (the physics of which is not entirely clear). The signal problem is heuristically at least as hard. In this thesis, we study the flow problem using classical fluid dynamics.

There is certainly no amenable global analytic solution to the general flow problem. However, a deeper insight can be gained by looking at various asymptotic regimes. Only a handful of authors have done so. Billingham & King [2] consider a model problem in which an infinite, initially straight interface between two inviscid fluids is advected in an initially uniform flow towards a semi-infinite thin, flat plate which is normal to the interface. There is no drainage mechanism, which allows the authors to investigate the factors that control the motion of a contact line over the idealised probe (and therefore the lagging contact line effect). Pearson [11] - [14] describes numerous approaches to combat many different areas of the problem; we discuss these at greater length as the appropriate regimes arise throughout this thesis.

One of the most interesting areas, from both an academic and industrial point of view, is the drainage mechanism in the neighbourhood of the probe that can lead to the drainage delay effect. Further, we have found no published literature which specifically addresses this problem. For these reasons, we focus our attention on it. For simplicity, we restrict ourselves to the 2-phase flow consisting of a single immiscible oil droplet approaching an axisymmetric probe through an infinite continuous water phase. We suppose that the cone of the probe joins smoothly onto a cylindrical upper body at a vertical distance D_C above the tip.

Since we are interested in the drainage mechanism in the neighbourhood of the probe tip, and the ratio of a probe diameter to an oil droplet diameter is typically very small, we consider the model problem in which the base far field flow supports an infinite flat interface moving steadily and uniformly with approach velocity $\mathbf{U}_\infty$. The axis of the probe is aligned with $\mathbf{U}_\infty$, while the unit normal $\mathbf{n}$ to the far-field interface is not in general aligned with $\mathbf{U}_\infty$. The acute angle between these vectors is the approach angle ϑ, which for most of this thesis we assume to be zero for simplicity. Figure 1.6 contains a schematic diagram of the initial set-up.

By considering an infinite interface, the drainage problem is made significantly more tractable and the results more widely applicable. However, it does not account fully for the phenomenon of grazing, for which we must consider the harder problem with a droplet.

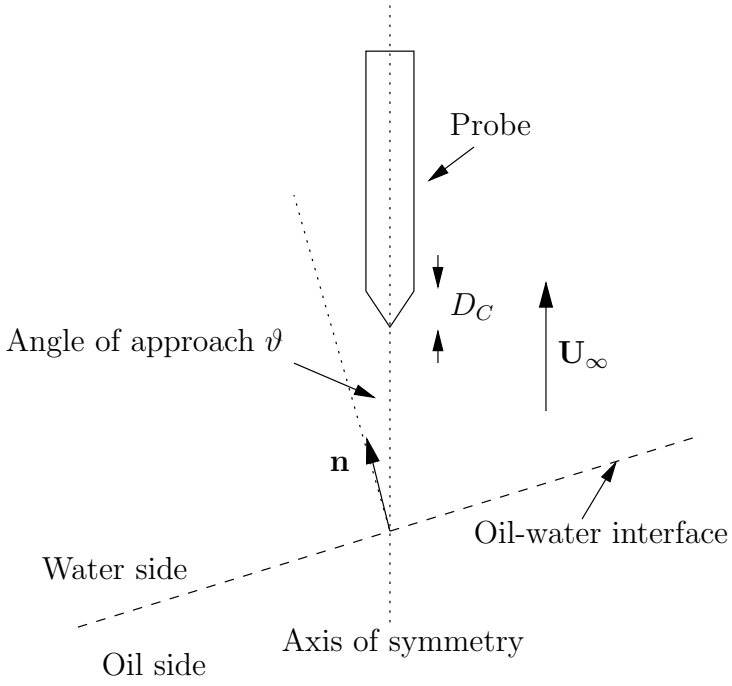


Figure 1.6: Initial configuration for the model problem.

For simplicity we limit the analysis to a *two-dimensional* geometry since the more realistic three-dimensional case should be qualitatively similar. In addition, we assume an *empirical rupture law*: the water film trapped between the probe and the interface thins until its minimum thickness reaches a characteristic critical value, typically a few hundred Angstroms, and then ruptures on a very short time-scale. Long-range inter-molecular (van der Waals) forces take over at such small length scales and are thought to be the destabilizing mechanism that causes the rapid film breakdown. It is proposed that rupture causes the formation of the characteristic 3-phase contact lines, which *either* move up the probe *or* "hang up" on the asperities or edges at which they formed. A more in-depth analysis is required to establish whether or not a residue of oil is left behind in the neighbourhood of the tip at rupture (which would spell disaster for the measurement principle). The most we can say intuitively is that this is unlikely if rupture begins at the tip, but becomes increasingly likely the further rupture begins up the probe.

Observe that the empirical rupture law determines the significance of the drainage delay effect. If the measurement neighbourhood N has maximum thickness h_{N}, with respect to the probe surface, and the film rupture thickness is h_{rup}, then the effect is significant if $h_{rup} \ll h_{\mathrm{N}}$.

Within the framework of the model problem we are motivated by the following two main problems.

(A) Given a particular probe shape, how does the interface drain in the neighbourhood of the probe?

(B) To optimise the shape of the probe so that the *drainage distance*, namely the vertical distance from the probe tip to the far-field interface at rupture, is minimized over given distributions of approach speeds $\mathbf{U}_\infty \in \Sigma$ and angles $\vartheta \in \Theta$.

Problem (B) is formulated by assuming that the signals are made as near to ideal as possible by minimizing the drainage distance. We consider the case of a normally approaching interface where $\Theta \equiv \{0\}$, but allow the approach speed to vary over the set of realistic values (typically 0.1 to 2.0 ms^{-1}).

1.3 Thesis structure

We begin in chapter 2 by nondimensionalising the governing equations to examine the relative sizes of the four forces acting: inertia, gravity, viscosity and surface tension. In chapter 3 we detail the resulting asymptotic regimes and approximations that may be used to decompose the drainage problem into more manageable sub-problems. For each, we briefly discuss possible methods of approach and relevant literature, and give a few elegant examples to illustrate the deep nature of the problem. In chapter 4 we diverge from our solution strategy to carry out an analysis of the drainage mechanism applicable to the case of a very slow moving oil droplet (around an arbitrarily shaped symmetric smooth probe). This is arguably the "worst" case from the point of view of the measurement principle, since such a droplet will take the longest time to rupture. We assume the system is in quasi-static equilibrium, so that inertia is negligible and a lubrication approach, driven by gravity and surface tension, is possible. In chapter 5 we return to one of the most important regimes introduced in chapter 3. We analyse the drainage mechanism around an arbitrarily shaped symmetric smooth probe, in the fully inviscid approximation, with surface tension and a density contrast. We conclude in chapter 6 by summarizing our results and discussing their implications for the industrial field. Finally we suggest some of the numerous extensions to this thesis which could be carried out in the future.

Chapter 2

Formulation of the problem

In this chapter we formulate and nondimensionalise the equations governing the full three dimensional problem. Clearly, these hold for all possible sub-problems, including the two dimensional model problem, with appropriate minor modifications to the boundary conditions at infinity.

2.1 Fundamental assumptions and the governing equations

We model the water and oil as immiscible, incompressible Newtonian viscous fluids and label their flow fields and physical properties with the subscripts 1 and 2, respectively. We assume their viscosities μ_1, μ_2 and densities ρ_1, ρ_2 are constant over the physical ranges under consideration. It is convenient to transfer the gravity dependence from the field equations to the boundary conditions by defining a *reduced* pressure p_i relative to the local hydrostatic pressure, thus

$$P_i = -\rho_i g z + p_i,$$

where P_i is the actual pressure, g is the acceleration due to gravity and z is the upward-pointing Cartesian coordinate along the axis of the probe. The Navier-Stokes equations for conservation of mass and momentum within each of the fluids are then

$$\nabla \cdot \mathbf{u_i} = 0, \tag{2.1}$$

$$\frac{\partial \mathbf{u_i}}{\partial t} + (\mathbf{u_i} \cdot \nabla)\mathbf{u_i} = -\frac{1}{\rho_i}\nabla p_i + \frac{\mu_i}{\rho_i}\nabla^2 \mathbf{u_i}, \tag{2.2}$$

where the gradient operator $\nabla = (\frac{\partial}{\partial x}, \frac{\partial}{\partial y}, \frac{\partial}{\partial z})$ and (x, y, z) are classical Cartesian coordinates, with origin O, say, at the probe tip.

Before rupture, the appropriate boundary condition on the probe surface S is the classical no-slip condition,

$$\mathbf{u_1} = \mathbf{0} \quad \text{on} \quad S. \tag{2.3}$$

After rupture, a contact line forms on the probe surface that requires an infinite stress to move under (2.3). To analyse moving contact lines (which we do not attempt here) it is

necessary to modify (2.3) to one of the many popular slip conditions; see for example Myers [9] for a brief discussion.

For the boundary conditions on the interface I, we assume that it is described by the single-valued equation $z = \eta(x, y, t)$ at time t. The kinematic condition, which says that a fluid particle that is initially on a free-surface remains on it, is then given by

$$\mathbf{u_1} = \mathbf{u_2} \quad \text{and} \quad w_1 = \eta_t + (\mathbf{u_1} \cdot \nabla)\eta \quad \text{on} \quad z = \eta. \tag{2.4}$$

For simplicity, we consider a constant surface tension model. In practice, the mixture is contaminated with naturally occuring pollutants, at least some of which will be surface active. The efficiency of the probe could crucially depend on the concentration of these surfactants and this should, in future, be tested experimentally and theoretically.

The stress condition on the interface is derived by considering the force balance on a small surface element and may be written

$$(\sigma\kappa_I + \Delta\rho g z)\mathbf{n_I} \quad = \quad (p_1 - p_2)\mathbf{n_I} - (\mu_1\mathbf{e_1} - \mu_2\mathbf{e_2}) \cdot \mathbf{n_I} \quad \text{on} \quad z = \eta, \tag{2.5}$$

where σ is the constant surface tension, κ_I is the curvature of the interface (positive at a point when the water domain is locally convex), $\Delta\rho = (\rho_1 - \rho_2)$ is the density difference, $\mathbf{n_I}$ is the unit normal vector to the interface that points into the water, and $\mathbf{e_i}$ are the classical rate of strain tensors.

The standard normal and tangential stress conditions are obtained by taking the dot product of (2.5) with $\mathbf{n_I}$ and $\mathbf{t_I}$, respectively, where $\mathbf{t_I}$ is any unit tangent vector to the interface. In the two-dimensional problem, in the (x, z) plane say, we choose the tangent vector pointing in the positive x direction.

The boundary condition at infinity for the full problem, and indeed, for any sub-problem involving the oil droplet, is given by

$$\mathbf{u_1} \to \mathbf{U}_\infty \quad \text{as} \quad |\mathbf{x}| \to \infty. \tag{2.6}$$

For the model interface problem this becomes,

$$\mathbf{u_1}, \mathbf{u_2} \sim \mathbf{U}_\infty \quad \text{and} \quad \eta - U_\infty t \sim x \tan\theta|_{\theta=0} = 0 \quad \text{as} \quad |\mathbf{x}| \to \infty, \tag{2.7}$$

without loss of generality, by appropriate orientation of the far field interface and appropriate choice of the time origin.

The specification of appropriate initial conditions for a well-posed problem is a non-trivial task; see for example Eames et al. [4] for a discussion appropriate to the fully inviscid case. However, since we are interested in the drainage mechanism in the neighbourhood of the tip just before rupture, it is sufficient to concern ourselves with locally valid solutions based on quasi-realistic initial conditions.

We comment that experiments carried out by SCR suggest that the wetability of the probe surface is crutial to the accuracy of the probe signals. The current interpretation of the probe physics is that there exists a permanent wetting layer on the probe surface, at least on oil-wet probes. This could dramatically change the boundary conditions on the probe "surface" for thin films of the non-wetting phase lying near the surface. Our analysis applies only to a clean probe.

2.2 Nondimensionalisation

We nondimensionalise with respect to the generic values determined by the outer bulk flow and the typical probe diameter D, by setting

$$\begin{aligned} \mathbf{x} &= D\,\mathbf{x}^*, \\ \mathbf{u}_\alpha &= U_\infty\,\mathbf{u}_\alpha{}^*, \qquad (\alpha = 1, 2, I), \\ p_\alpha &= \rho_\alpha U_\infty{}^2\, p_\alpha{}^*, \quad (\alpha = 1, 2), \\ \kappa_I &= \tfrac{1}{D}\,\kappa_I{}^*, \\ t &= \tfrac{D}{U_\infty}\,t^*. \end{aligned} \tag{2.8}$$

The field equations (2.1) and (2.2) become, upon dropping stars,

$$\nabla \cdot \mathbf{u_i} = 0, \tag{2.9}$$

$$\frac{\partial \mathbf{u_i}}{\partial t} + (\mathbf{u_i} \cdot \nabla)\mathbf{u_i} = -\nabla p_i + \frac{1}{\mathrm{Re}_i}\nabla^2 \mathbf{u_i}, \tag{2.10}$$

where the ratio of inertial to viscous forces in each of the fluids is given by the corresponding Reynolds number

$$\mathrm{Re}_i = \frac{\rho_i U_\infty D}{\mu_i}.$$

The no-slip and kinematic boundary conditions (2.3), (2.4) are unchanged. The normal and tangential free surface stress conditions, given by (2.5), become

$$\kappa_I + \mathrm{Bo}\, z = (\mathrm{We}_1\, p_1 - \mathrm{We}_2\, p_2) - \mathbf{n_I} \cdot (\mathrm{Ca}_1\, \mathbf{e_1} - \mathrm{Ca}_2\, \mathbf{e_2}) \cdot \mathbf{n_I} \text{ on } z = \eta, \tag{2.11}$$

$$0 = \mathbf{t_I} \cdot (\mathrm{Ca}_1\, \mathbf{e_1} - \mathrm{Ca}_2\, \mathbf{e_2}) \cdot \mathbf{n_I} \text{ on } z = \eta, \tag{2.12}$$

where the ratios of inertial and viscous forces to surface tension in each of the fluids are given by the Weber and Capillary numbers,

$$\mathrm{We}_i = \frac{\rho_i U_\infty^2 D}{\sigma},\ \mathrm{Ca}_i = \frac{\mu_i U_\infty}{\sigma},$$

respectively, while the ratio of gravity to surface tension is given by the Bond number

$$\mathrm{Bo} = \frac{\Delta\rho g D^2}{\sigma}.$$

The boundary conditions at infinity are exactly the same as the dimensional ones, (2.6) and (2.7), except with $\mathbf{U}_\infty$ replaced by (0,0,1).

2.3 The dimensionless parameter groups

Typical dimensions and fluid properties for production logging in the field are displayed in table 2.1. The density ratio $r = \rho_1/\rho_2$ and viscosity ratio $m = \mu_1/\mu_2$ are typically $O(1)$, so observing

$$\mathrm{Re}_1 = \frac{r}{m}\,\mathrm{Re}_2,\ \mathrm{We}_1 = r\,\mathrm{We}_2,\ \mathrm{Ca}_1 = m\,\mathrm{Ca}_2,$$

we use representative values ρ, μ for the dimensionless parameters.

Name	Symbol	Typical values	Units
Water density	ρ_1	1000	Kg m^{-3}
Oil density	ρ_2	750 -1000	Kg m^{-3}
Density difference	$\Delta\rho$	0 - 250	Kg m^{-3}
Density ratio	r	0.75 - 1.0	No units
Water viscosity	μ_1	1.0×10^{-3}	Kg $\mathrm{m}^{-1}\mathrm{s}^{-1}$
Oil viscosity	μ_2	1.0×10^{-3} - 3.0×10^{-3}	Kg $\mathrm{m}^{-1}\mathrm{s}^{-1}$
Viscosity ratio	m	1.0 - 3.0	No units
Surface tension	σ	0.005 - 0.05	N m^{-1}
Velocity	U_∞	0.1 - 2.0	m s^{-1}
Probe diameter	D	0.2×10^{-3} - 1.2×10^{-3}	m
Droplet diameter	D_D	1.0×10^{-3} - 7.0×10^{-3}	m
Pipe diameter	D_{pipe}	0.1 - 0.5	m

Table 2.1: Typical dimensions and fluid properties for production logging.

There are four forces acting whose ratios give six dimensionless parameters of which a minimum of three are independent. Our nondimensionalisation introduced four and a "basis" may be built from them by taking the Bond number and any two of those remaining, since

$$\mathrm{We} = \mathrm{Ca} \cdot \mathrm{Re}.$$

Nevertheless, we list all six parameters in table 2.2, together with their typical values. Note that it is the reduced Froude number $\mathrm{Fr}^* = \Delta\rho/(\rho\,\mathrm{Fr}^2)$ that appears above, where $\mathrm{Fr} = U_\infty/\sqrt{g\,D}$ is the classical Froude number.

Name	Symbol & formula	Force ratio	Typical values
Reynolds	$Re = \frac{\rho U_\infty D}{\mu}$	$\frac{\text{inertial}}{\text{viscous}}$	5.0 - 2400
Weber	$We = \frac{\rho U_\infty^2 D}{\sigma}$	$\frac{\text{inertial}}{\text{capillary}}$	0.03 - 960
Capillary	$Ca = \frac{\mu U_\infty}{\sigma}$	$\frac{\text{viscous}}{\text{capillary}}$	0.002 - 0.6
Bond	$Bo = \frac{\Delta\rho g D^2}{\sigma}$	$\frac{\text{gravity}}{\text{capillary}}$	0 - 0.72
Froude	$Fr^* = \frac{\rho U_\infty^2}{\Delta\rho\, g\, D}$	$\frac{\text{inertial}}{\text{gravity}}$	15.0 - ∞
Stokes	$St = \frac{\Delta\rho\, g\, D^2}{\mu U_\infty}$	$\frac{\text{gravity}}{\text{viscous}}$	0 - 36.0

Table 2.2: The dimensionless parameter groups.

The generic case has $\mathrm{Re} \gg 1$, $\mathrm{Ca} \ll 1$, $\mathrm{Bo} \ll 1$ and $\mathrm{Fr}^* \gg 1$, with St and We varying from very small to moderately large (to differing degrees). This corresponds to the most common situation in the field where the pipe velocity is high ($U_\infty \sim 1\,\mathrm{ms}^{-1}$). We have therefore found the following.

(i) Inertial forces dominate over viscous forces, at least over length scales greater than or equal to the probe diameter, while surface tension dominates over gravity over all smaller length scales.

(ii) Inertial forces dominate over gravity and surface tension dominates over viscous forces, on all length scales.

(iii) The Stokes number determines the balance between the weak pair, namely viscous and gravity forces, on all length scales.

(iv) The Weber number determines the balance between the dominant pair, namely inertial and capillary forces, on the length scale of a probe diameter.

The actual length scales over, which the pairs of forces in (i) and (iv) balance, are found by solving

$$\mathrm{Re} = 1,\ \mathrm{Bo} = 1,\ \mathrm{We} = 1$$

for D, using typical vales for ρ, U_∞, μ, σ, $\Delta\rho$ and g. The results are the viscous D^V, capillary D^C and inertial D^I lengths, respectively.[1] We find

$$\begin{array}{ccccccccc} \text{viscous} & \sim & \text{inertia} & \Leftrightarrow & D^V & \sim & 10^{-7} - 10^{-6} & \text{m}, \\ \text{capillary} & \sim & \text{gravity} & \Leftrightarrow & D^C & \sim & 10^{-3} - \infty & \text{m}, \\ \text{inertia} & \sim & \text{capillary} & \Leftrightarrow & D^I & \sim & 10^{-5} - 10^{-3} & \text{m}. \end{array} \tag{2.13}$$

For the generic case (where $U_\infty \sim 1\,\mathrm{ms}^{-1}$), we conclude that inertial forces dominate over viscous forces at all length scales above about 1μm. We expect laminar flow on the probe scale, with an outer inviscid flow that matches into thin viscous boundary layer flow on the probe surface and on each side of the interface.[2] As the interface approaches the probe the boundary layers will interact and merge, which may be analysed by considering the appropriate asymptotic regimes (see chapter 3). We can also say that inertial forces dominate over interfacial tension at all length scales above about 1 mm (that is, about a typical probe diameter), which in its turn, dominates over gravity over all smaller length scales.

Hence the simplest relevant model is fully inviscid (so that momentum flux balances pressure gradients), with the Laplace-Young equation on the interface (so that surface tension balances the pressure jump across the interface). Other useful asymptotic regimes and approximations are the subject of the following chapter.

[1] We follow Pearson [11] in this interpretation.

[2] In order to satisfy the no-slip and zero shear conditions, respectively.

Chapter 3

Asymptotic regimes

3.1 Preliminaries

In this chapter we consider the natural asymptotic regimes and approximations that decompose the two dimensional model problem with a normally approaching interface. The idea is that, as the interface gradually approaches the probe, we pass through a series of asymptotic regimes over which different physical effects balance. Thus, the formidable full initial value model problem for the evolution of the interface is decomposed into a number of more manageable sub-problems. The aim is touse the "final" conditions from the previous regime as initial conditions for the subsequent one. Clearly, between these distinguished regimes are intermediate limits where all the effects enter at once. For each we suggest possible methods of approach and relevant literature.

First, we establish the thickness of the thin viscous boundary layers on the probe and on each side of the interface, say Δ_p and Δ_I, respectively. The universal result on the rigid probe surface is simply

$$\Delta_p \quad = \quad O\Big(\frac{D}{\sqrt{Re}}\Big).$$

However, there is is no geometrical length scale associated with an infinite interface, so we use the "natural" length scale determined by balancing the dominant forces on the interface. This is simply the inertial length,

$$D^I \quad = \quad \frac{\sigma}{\rho {U_\infty}^2}.$$

The boundary layer thickness on a free surface depends intricately on the shape of the interface and on the form of the flow fields (see for example Batchelor [1], section 5.14). The most we can say in general is that

$$\Delta_I \quad \leq \quad O\Big(\frac{D^I}{\sqrt{Re_I}}\Big),$$

where the Reynolds number is

$$Re_I \; = \; \frac{\rho\, U_\infty\, D^I}{\mu}.$$

With the typical values displayed in table 2.1 we find,

$$\begin{aligned} \Delta_p &\sim 10^{-5} - 10^{-4}\,\mathrm{m}, \\ \Delta_I &\lesssim 10^{-6} - 10^{-4}\,\mathrm{m}. \end{aligned}$$

Thus, the boundary layer on the interface is typically thinner than on the probe surface.

As the interface approaches the probe, the dimensional distance from the probe tip to the interface along the axis of symmetry, H say, decreases from "infinity" to zero, passing through Δ_p and Δ_I. It is therefore natural to characterise the time evolution by the relative size of H and Δ_p.

We remark that if we had considered the oil droplet problem, the free-surface boundary layer thickness would be $O(D_D/\sqrt{Re_D})$, with the Reynolds number Re_D based on a typical droplet diameter D_D. With the typical values of table 2.1, the resulting dimensional boundary layer thickness is typically 10^{-5} - 10^{-4}m. With appropriate modifications, nearly all of the results and observations hold for a non-normally approaching interface or droplet, as well as in three dimensions.

3.2 Asymptotic regimes

3.2.1 Early stage of approach

Here we suppose $H \gg D$ so that the interface is sufficiently far from the probe that they do not interact. The local flow near to each of them is essentially the same as if they were entirely isolated. The relevant subregimes are therefore steady, laminar, high-Reynolds-number flow of (i) the single water phase past the probe and (ii) both the phases separated by an infinite initially flat interface.

The first of these is a classical boundary layer problem. An outer inviscid flow is matched into a thin viscous boundary layer of thickness Δ_p on the probe surface, which is needed to satisfy the no-slip condition there. For a modest Reynolds number and a sufficiently smooth probe surface (with total curvature monotonically decreasing with distance from the tip) there is no separation of the boundary layer. Separation is most likely to occur for more blunt probe cones near to the where the cone joins onto the cylindrical upper body.

There are many relevant solutions in the literature, at least for flow local to the tip. For example, flow past a semi-infinite flat plate and a wedge are dealt with in detail by O'Neil & Chorlton [3] and Ockendon & Ockendon [10]. Further, flow past a semi-infinite flat plate and a parabola are discussed in the context of optimal coordinates[1] in Van Dyke [17].

We now consider the second regime, namely the propagation of an infinite, initially flat interface between two immiscible liquids. The appropriate trivial solution has a flat interface and $\mathbf{u_i} = \mathbf{U}_\infty$ throughout. Of particular interest is the stability of this solution to small perturbations, since an unstable interface may undergo significant deformation over the time it takes to reach the probe. The interface will develop boundary layers when subjected to small perturbations, in order to satisfy both of the free surface stress conditions. It is

[1] That is, optimal in the Kaplun sense; see [8]

reasonable to expect that surface tension will stabilize the interface, at least for sufficiently small Weber number. A natural expansion parameter might be $\epsilon = h_0/D_I$ where h_0 is a typical vertical displacement, taken to be small relative to the boundary layer thickness Δ_I.

We remark that the corresponding regime for the more realistic three dimensional droplet problem is simply an isolated droplet rising steadily in a flow with uniform velocity at infinity. For sufficiently high surface tension (small Weber number) the droplet remains approximately spherical and there are two classical solutions in the literature for different asymptotic limits. These are Hadamard's solution for the zero Reynolds and Capillary number limit (see Batchelor [1]), and a modified Hill's spherical vortex solution for an inviscid rotational flow with no density contrast between the fluids (see Pearson [12]). The first is certainly not applicable to our high-Reynolds number flow, while the second predicts a terminal rise velocity that is close to observed values. In the large Weber number case, the droplet deforms into a "spherical cap". The boundary layers separate at the edges resulting in a trailing wake.

3.2.2 Initial deformation of the interface

As H/D decreases to values of order unity, the interface will begin to deform due to the presence of the probe. Since $H \geq D \gg \Delta_P$ the boundary layers are thin relative to the distance of the interface from the probe. The simplest relevant flow model is therefore fully inviscid.

For sufficiently small Weber and Bond numbers the deformation will be small, at least until $H/D = O(1)$. In the large Weber and small Bond number limits there is no pressure jump across the interface (by (2.11)). The interface is therefore indistinguishable from an appropriately chosen streakline[2] in the corresponding single-phase flow past the probe, and the deformation will be large. For intermediate Weber numbers the behaviour of the interface varies between these extremes.

For large Weber numbers and no density contrast, a deeper understanding could hopefully be gained by consideration of a small perturbation to the "infinite" Weber number single-phase streakline flow. A natural expansion parameter is the reciprocal of the Weber number.

Alternatively, the fully inviscid flow with surface tension and non-zero density contrast could be tackled numerically using the boundary integral method. The method is based on discretising a boundary integral formulation of the problem, which is derived by applying Green's second theorem in the plane to each of the fluid domains, with the fundamental solution of Laplace's equation as the auxillary or Green's function. Then, given sufficient regularity conditions at infinity, the domain integrals are eliminated and the result is a relation between the potential at a point in the fluid domain, or on its boundary, to a weighted integral of the potential and the flux on the boundaries. The reader is referred to Billingham & King [2] for a detailed formulation of the method that is relevant to this regime.

[2] A streakline is simply a marked line/plane of fluid in two/three dimensional flow.

3.2.3 The thinning phases

As the interface is dragged past the probe by the far field bulk flow, it forms a film on the probe surface in some neighbourhood of the tip. For sufficiently large times, $H \ll D$ and the aspect ratio $\epsilon = H/L$ of the film is small, where the probe diameter D and the length of the film L are not necessarily of the same order.

The relative size of the film thickness H and the boundary layer thickness on the probe Δ_p, identifies three distinct regimes.

(i) If $\Delta_p \ll H$, then the thin viscous boundary layers on the probe surface and the near side of the interface do not interact and the flow in the thin film is dominated by inertial forces.

(ii) If $\Delta_p \sim H$, then the viscous boundary layers on the probe surface and on the near side of the interface have "merged" and the flow in the thin film is driven by both inertial and viscous forces.

(iii) If $\Delta_p \gg H$, then the thin film lies well inside what was the viscous boundary layer on the probe surface and is dominated by viscous forces.

This results in three different "thinning" regimes in the layer, namely inertial, inertial/viscous and viscous dominated flow (corresponding to (i), (ii) and (iii) respectively). The governing momentum equations in each are simply the Euler, Prandlt boundary layer and Stokes flow equations, respectively.

In each regime, the flow on the oil side of the interface is governed by Prandtl's boundary layer equations, which must be matched to the outer inviscid flow in the oil. Since the aspect ratio is small, the pressure is constant across the thin film *and* the boundary layer, to leading order in ϵ and $1/\sqrt{Re_I}$. Further, to this order of magnitude, the pressure in the boundary layer is equal to the external inviscid pressure in the oil, $p_{inv}(s, 0, t)$ say, while in the thin film it is given by the normal stress condition (2.11) with $p_2 = p_{inv}(s, 0, t)$.

Motivated by the above observations, we conjecture that in each regime the flow domain can be decomposed into separate regions. The "outer" problem being on a scale on which the film thickness is zero. To avoid a force singularity the interface must meet a smooth probe surface tangentially, resulting in a special kind of moving contact line problem. The Navier slip condition, or some other more elaborate model, must be introduced to remove the force singularity that results from the no-slip assumption. The contact line interacts with the viscous boundary layers in a way which is not totally clear. The reader is referred to Pearson [11] for a detailed discussion of this problem. We remark that a deeper insight can be gained by considering the fully inviscid model. This is the subject of chapter 5.

Of most interest is the *relative contribution of each of the thinning phases to the drainage delay effect*. The rupture time scale and the drainage distance provide good measures on which to base the comparisons. The analysis could be simplified by taking an initially uniform film profile, since "there is a strong chance that any initial position for the interface that is monotonically increasing away from the forward stagnation point would lead with time to a universal asymptotic form," Pearson [14].

3.2.4 Single-phase flows

The most simple models are those based on single-phase flows in which surface tension and gravity are ignored, so that the interface is indistinguishable from an appropriately chosen streakline. Consideration of the thinning phases discussed above shows that relevant single-phase flows are those with zero, small or large viscosity, corresponding to purely inviscid, high-Reynolds-number and purely viscous flow, respectively.

For each of these flows, it is easy to show that smooth probe shapes have streaklines that do not reach the probe in finite time. Indeed, the minimum distance from the probe tip to the interface is, in general, some exponentially decaying function of time whose rate increases with the flow velocity at infinity.[3] This is not the case for non-smooth probe profiles, for which the behaviour of the streaklines is not immediately clear. It is therefore instructive to consider the motion of the streaklines in the single-phase flow past the simplest of non-smooth probe shapes: the wedge.

Single-phase flow past a wedge

We consider symmetric flow past a two-dimensional wedge with apex angle $2\pi(1-\beta)$. We allow β to vary over $(0,1]$ with $\beta = 1/2$ and $\beta = 1$ corresponding to the special cases of a wall and a semi-infinite flat plate, respectively. The configuration is sketched in figure 3.1.

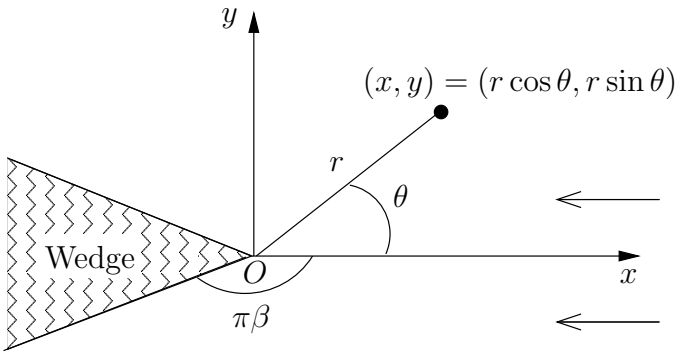


Figure 3.1: Cartesian $O(x,y)$ and polar $O(r,\theta)$ coordinates for the wedge.

We nondimensionalise exactly as in the previous chapter, identifying U as the flow velocity on the axis of symmetry at a distance D from the tip. We consider separately purely inviscid, high-Reynolds-number and purely viscous flow. Except for the special cases, there is no solution that matches with uniform flow at infinity. We therefore consider the relevant symmetric flow in the neighbourhood of the vertex, which is consistent with our nondimensionalization.

[3] Given sufficient smoothness conditions on the probe surface, the fluid velocity is bounded throughout the flow domain and there is only one stagnation point at the tip. Since particle paths can only cross at stagnation points or singular points, it is sufficient to consider the flow near to the tip. The local analysis is essentially the same as normal flow toward a flat infinite wall, for which there is a solution of the full Navier-Stokes equations; see below for the analysis.

1. The inviscid case

We use a velocity potential/stream function approach to study the flow which is assumed to be incompressible and irrotational. The unique symmetric solution with speed -1 at $(1,0)$ and zero normal velocity on the surface of the wedge, obtained by conformally mapping from uniform flow past an infinite plate, has complex potential,

$$w(z) = -\tfrac{\beta}{1+\beta} z^{\frac{1+\beta}{\beta}}, \tag{3.1}$$

where $z = x + iy$ in the classical notation of complex variable theory.

Let $\mathbf{x}(t) = (r(t)\cos\theta(t), r(t)\sin\theta(t))$ be the position vector, at time t, of the fluid particle starting at $\mathbf{x_0} = (r_0\cos\theta_0, r_0\sin\theta_0)$, at time $t = 0$. It is straight forward to show that the particle path is given by,

$$\begin{array}{rcl} \int_{\theta_0}^{\theta(t)} \frac{1}{[\sin(\zeta/\beta)]^{2\beta}}\, d\zeta & = & r_0^{\frac{1-2\beta}{\beta}} [\sin(\theta_0/\beta)]^{1-2\beta}\, t, \\ r(t) & = & r_0 \left[\frac{\sin(\theta_0/\beta)}{\sin(\theta(t)/\beta)}\right]^{\frac{1}{\beta}}, \end{array} \tag{3.2}$$

provided $\theta_0 \neq 0$.[4] This corresponds to the motion of the *centre point*, $(h(t), 0)$ with $h(0) = h_0 > 0$ say, and is given by,

$$h(t) = \begin{cases} \left(h_0^{\frac{2\beta-1}{\beta}} + (\frac{1-2\beta}{\beta})t\right)^{\frac{\beta}{1-2\beta}}, & \beta \in (0, 1/2), \\ h_0 \exp(-t), & \beta = 1/2, \\ \left(h_0^{\frac{2\beta-1}{\beta}} - (\frac{2\beta-1}{\beta})t\right)^{\frac{\beta}{2\beta-1}}, & \beta \in (1/2, 1]. \end{cases} \tag{3.3}$$

The centre point hits the origin in finite time if, and only if, the apex angle is acute, i.e. $\beta \in (1/2, 1]$. If the apex angle is obtuse , i.e. $\beta \in (0, 1/2)$, then the centre point tends to the origin algebraically in time. In the special case of a wall, i.e. $\beta = 1/2$, the centre point tends to the wall exponentially in time. The drainage distance,[5] with respect to dimensional uniform flow at velocity U, is easily found for the acute-angled wedge, and tends to zero with this angle (as expected).

The motion of a streakline with arbitrary initial position is found by following all of its constituent fluid particles using (3.2) and (3.3). Of particular interest is what happens when a streakline hits the vertex of an acute-angled wedge. The apex is a stagnation point of the flow, so naïve reasoning might lead us to believe that the streakline "hangs up" on the apex, resulting in a *pinned contact line*. It is therefore surprising to find that the wedge instantaneously penetrates the streakline. To explore the manner in which it does so, consider the streakline that starts on the positive y axis, so that $r = s$ and $\theta = \pi/2$ for $s \in [0, \infty)$ at $t = 0$. This should give us the local behaviour of *any* streakline which hits the wedge normally.

[4] The second equation in (3.2) is simply the parametric equation of the streamline through $\mathbf{x_0}$.

[5] Recall that this is the perpendicular distance from the probe tip to the far field interface at rupture.

By (3.2) we have,

$$s \;=\; \Big[\tfrac{F(\theta)}{t}\Big]^{\frac{\beta}{1-2\beta}}\Big(\sin(\tfrac{\pi}{2\beta})\Big)^{-\beta} \quad \text{and} \quad r \;=\; s\Big(\tfrac{\sin(\pi/2\beta)}{\sin(\theta/\beta)}\Big)^{\beta}, \tag{3.4}$$

where,

$$F(\theta) \;=\; \tfrac{\beta}{2}\Big[B(\cos^2(\theta/\beta),1/2,1/2-\beta) \;-\; B(\cos^2(\pi/2\beta),1/2,1/2-\beta)\Big],$$

and B is Euler's Beta function,

$$B(z,a,b) = \textstyle\int_0^z \zeta^{a-1}(1-\zeta)^{b-1}d\zeta.$$

Eliminating s from (3.4),

$$r \;=\; \Big[\tfrac{t}{F(\theta)}\Big]^{\frac{\beta}{1-2\beta}}\Big(\sin(\tfrac{\theta}{\beta})\Big)^{\beta}. \tag{3.5}$$

Since $\beta > 1/2$, $r \to 0$ (i.e. the fluid particle which starts at the origin) corresponds to $F(\theta) \to \infty$, and this happens as $\theta \to \beta\pi$. In fact, the asymptotic behaviour of r near $\theta = \beta\pi$ is,

$$r \sim \Big(\tfrac{(2\beta-1)t}{\beta}\Big)^{\frac{\beta}{1-2\beta}}\Big[1 \;+\; O\Big((\pi-\tfrac{\theta}{\beta})^{2\beta-1}\Big)\Big]. \tag{3.6}$$

This shows quantitatively how the contact line starts to climb up the wedge.

Figure 3.2 illustrates the motion of the streakline that starts on $x = 1$ for a 45° apex-angle. The time step between the profiles is 0.1 units. The equations for the particle paths (3.2) were integrated using the Euler method with a much smaller time-step. We see that the streakline lags behind in the neighbourhood of the tip.

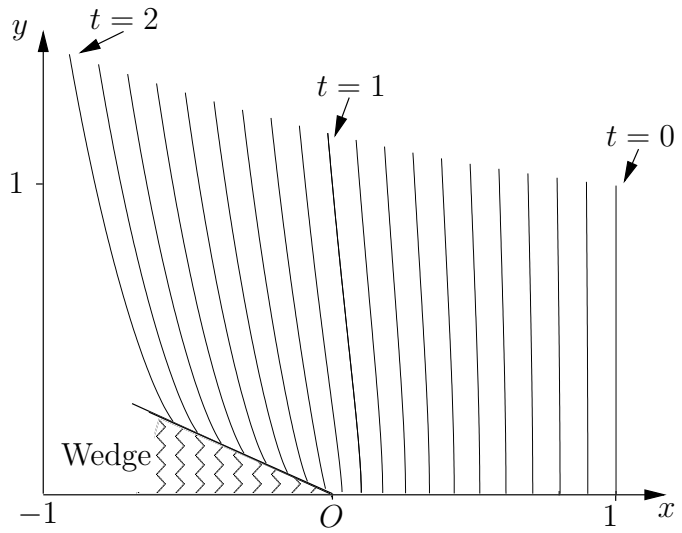


Figure 3.2: Motion of a streakline past a wedge.

■

2. The high-Reynolds-number case

We consider the high-Reynolds-number flow driven by exactly the same pressure gradient at infinity as in the purely inviscid flow detailed above. The introduction of viscosity necessitates the implementation of the no-slip boundary condition on the wedge. The inviscid flow is the leading order solution to a regular perturbation in the small parameter $1/\sqrt{\mathrm{Re}}$, where the Reynolds number is given by

$$\mathrm{Re} = \frac{\rho U D}{\mu} \gg 1,$$

in the usual notation. Clearly, this solution has the right behaviour in the far field but fails to satisfy the no-slip condition. This *outer* solution is therefore valid everywhere except in a thin boundary layer on the wedge, which must be introduced to determine the *correct* leading order momentum equations there and to satisfy the no-slip condition. The correct *inner* leading order momentum equations are Prandtl's boundary layer equations, found by looking in a neighbourhood of thickness $O(1/\sqrt{\mathrm{Re}})$ around the wedge, in order to retain the viscous term in the tangential momentum equation. These equations are given by[6]:

$$\begin{aligned} uu_s + wu_n &= -p_s + \nu u_{nn}, && (3.7)\\ 0 &= -p_n, && (3.8)\\ u_s + w_n &= 0, && (3.9) \end{aligned}$$

where s is the distance along the upper side of the wedge from the tip[7], n is the normal distance from this side, (u, w) is the flow field relative to the transformed Cartesian frame (s, n), p is the pressure field and the dynamic viscosity $\nu = \mu/\rho$. We emphasize that, for an acute apex-angle, this coordinate system is not optimal in the Kaplun sense (see Kaplun [8]), although it results in a uniformly valid solution in the boundary layer except near the tip. For the special case of a wall[8], this coordinate system is certainly optimal, indeed, the resulting *stagnation point* solution solves the full Navier-Stokes equations.

The no-slip condition on the wedge is

$$u = w = 0 \quad \text{on} \quad n = 0. \tag{3.10}$$

The matching condition connecting the inner boundary layer solution to the outer inviscid solution is

$$(u, w) \sim (\mathcal{U}, 0) \quad \text{as} \quad n \to \infty, \tag{3.11}$$

where $\mathcal{U}(s)$ is the inviscid slip velocity on the wedge given by

$$\mathcal{U}(s) = s^{\frac{1}{\beta}}. \tag{3.12}$$

By (3.9), the pressure is constant across the boundary layer, $p = p(s)$. Hence, applying Bernoulli's theorem to the streamline on the wedge in the outer flow field, we deduce that

[6] See for example O'Neil & Chorlton [3]

[7] By symmetry, it is sufficient to consider the flow in $y > 0$ only.

[8] This is of particular interest because it is exactly the flow field near to the tip that occurs in high-Reynolds-number flow past any smooth ended probe.

$p_s = -\mathcal{U}\mathcal{U}_s$. Defining the stream function $\psi(s,n)$ by $u = \psi_n$ and $w = -\psi_s$, the inner problem (3.8) through (3.11) becomes:

$$\begin{aligned} \psi_n\psi_{sn} - \psi_s\psi_{nn} &= \mathcal{U}\mathcal{U}_s + \nu\psi_{nnn}, \\ \psi = \psi_n &= 0 \quad \text{on} \quad n = 0, \\ \psi &\sim \mathcal{U}(s)n \quad \text{as} \quad n \to \infty. \end{aligned} \tag{3.13}$$

Seeking a similarity solution of the form

$$\psi(s,n) = \mathcal{U}(s)\xi(s)f(\eta) \quad \text{where} \quad \xi(s) = \sqrt{\tfrac{2}{\mathrm{Re}}}\tfrac{2\beta}{1+\beta}s^{\frac{\beta-1}{2\beta}} \quad \text{and} \quad \eta(s,n) = \tfrac{n}{\xi(s)},$$

we find that f satisfies the Falkner-Skan equation (see for example O'Neil & Chorlton [3]),

$$f''' + ff'' + \tfrac{2}{1+\beta}[1 - (f')^2] = 0, \tag{3.14}$$

in which prime denotes differentiation with respect to η. The boundary conditions become

$$f(0) = f'(0) = 0 \quad \text{and} \quad f'(\infty) = 1. \tag{3.15}$$

The nonlinear ordinary differential equation (3.14), together with the boundary conditions (3.15), may be solved by numerical methods to any desired degree of accuracy for any $\beta \in (0,1]$; see for example Rosenhead [15]. The results may then be used to construct the streakline motion *within* the boundary layer.

For simplicity, we consider the special case of stagnation point flow in which $\beta = 1/2$. Observing that $s \equiv y$ and $n \equiv x$, it is convenient to work with the standard Cartesian coordinates (x,y). The fluid velocity is given by

$$\mathbf{u} = (-f(x), yf'(x)),$$

so the particle path $(x(t), y(t))$, through (x_0, y_0) at $t = 0$ say, is defined by

$$\tfrac{dx}{dt} = -f(x) \quad \text{and} \quad \tfrac{dy}{dt} = yf'(x).$$

The solution is simply,

$$\textstyle\int_{x(t)}^{x_0} \frac{d\eta}{f(\eta)} = t \quad \text{and} \quad y(t) = \frac{y_0 f(x_0)}{f(x)}.$$

As mentioned above, this yields an exact solution of the Navier-Stokes equations, the so-called stagnation point solution. We deduce that the parametric equation of the streakline that initially lies on the curve $(x(\lambda), y(\lambda))$ for $\lambda \in \Lambda$ is given by,

$$\textstyle\int_{x(\lambda,t)}^{x(\lambda)} \frac{d\eta}{f(\eta)} = t \;\text{ and }\; y(\lambda,t) = \frac{\lambda f(x(\lambda))}{f(x(\lambda,t))} \quad \text{for} \;\; \lambda \in \Lambda.$$

It may be shown that $f''(\eta) \sim a\eta^2$ as $\eta \to 0$, for some $a > 0$. This implies that all points of any streakline approach the wall exponentially in time.

■

3. The viscous case

Here we consider the opposite extreme in which inertia is negligible. In polar coordinates the stream function ψ is defined to be such that

$$\mathbf{u} = \frac{1}{r}\frac{\partial \psi}{\partial \theta}\hat{\mathbf{r}} - \frac{\partial \psi}{\partial r}\hat{\boldsymbol{\theta}},$$

where $\mathbf{u}$ is the velocity field and $\hat{\mathbf{r}}$, $\hat{\boldsymbol{\theta}}$ are the unit radial and angular vectors, respectively.

The momentum equations reduce to the biharmonic equation for ψ, to which we add the no-slip condition on the wedge and the symmetry condition on the centre line:

$$\begin{aligned} \nabla^4 \psi = 0 \qquad & \text{for} \qquad 0 < \theta < \beta\pi, \\ \psi = \psi_\theta = 0 \qquad & \text{on} \qquad \theta = \beta\pi, \\ \psi = \psi_{\theta\theta} = 0 \qquad & \text{on} \qquad \theta = 0. \end{aligned} \tag{3.16}$$

Seeking a separable solution of the form $\psi = f(\theta) r^{n+1}$ or $\psi = f(\theta) r^{n+1} \log r$, with $n > 0$ to satisfy the no-slip condition at the vertex, we find,

$$\psi = \begin{cases} r^{n+1}[A\cos(n+1)\theta + B\sin(n+1)\theta + C\cos(n-1)\theta + D\sin(n-1)\theta], & n \neq 0, \\ r^2(1 + E\log r)[F\cos 2\theta + G\sin 2\theta + H\theta + I], & n = 1, \end{cases}$$

where $A, B, \ldots, I$ are arbitrary constants. Applying the boundary conditions results in a condition (on n) for there to exist a non-trivial solution (for each $\beta \in (0, 1]$). The special case, where $n = 1$, has a non-trivial solution if, and only if,

$$\tan(2\beta\pi) = 2\beta\pi. \tag{3.17}$$

This transcendental equation has a unique solution $\beta_c \in (1/2, 3/4]$, corresponding to an apex angle of about $102.5°$. When $n \neq 1$, the condition becomes,

$$\sin(2n\beta\pi) = n\sin(2\beta\pi). \tag{3.18}$$

The positive roots of (3.18), not equal to unity, determine the possible modes of the separable solution for each apex angle. Observe that β is a bifurcation parameter and the number, type and location of the roots vary with it in a continuous manner; see table 3.1.

β	Root properties
$1/2$	Simple roots at $n = 2, 3, 4, 5, 6, \ldots$.
$(1/2, \beta_c)$	Finite number of simple roots with $n^* > 1$.
β_c	Double root at $n = 1$.
$(\beta_c, 1)$	Finite number of simple roots with $n^* < 1$.
1	Simple roots at $n = 1/2, 3/2, 2, 5/2, 3, 7/2, 4, \ldots$.

Table 3.1: The positive root(s) of (3.17) for $n = 1$ and of (3.18) for $n \neq 1$.

Of most interest is the behaviour of the mode corresponding to the smallest positive root, since this determines the fastest possible rate at which the centre point can tend to the vertex. We denote this root by $n^*(\beta)$. The function $\beta \to n^*(\beta)$ is continuous and monotonic

decreasing on $[1/2, 1]$, with $n^*(1/2) = 2$, $n^*(1) = 1/2$ and a point of inflection at $\beta = \beta_c$ where $n^* = 1$, corresponding to the double root.[9]

It is clear that the centre point hits the origin in a finite time if and only if $n^* < 1$, and in this case the convergence is algebraic. If $n^* = 1$, the convergence is exponential, while, if $n^* > 1$, the convergence is again algebraic.

We conclude that an apex angle less than about 102.5° is necessary for a streakline to reach the vertex in finite time. Further, an analysis similar to the inviscid case shows that the streakline will then hang up on the apex. The reason for this is the application of the no-slip condition on the surface of the wedge.

In the model problem, the final stages of rupture are inevitably dominated by viscous effects, because the no-slip condition (2.3) guarantees that the flow velocity is small sufficiently close to the probe surface. The above analysis gives us a criterion for efficient film rupturing, namely that the apex-angle should be as small as possible and at least less than 102.5°.

■

Conclusion

We conclude that, neglecting surface tension and the density difference, a large number of interesting and useful analytic solutions could be found simply by tracing streaklines in a single-phase flow. Many such solutions may be found in the literature, and we refer the reader to the related problem of "drift", considered by Eames et al. [4], as an illustration of the difficulties that can occur in unbounded flows past objects.

3.3 Summary

We have briefly discussed the asymptotic regimes that decompose the model drainage problem. Ideally, each would be analysed in turn, so as to build up a comprehensive picture of the significant factors that influence the drainage delay effect. However, even the simplest thinning regime results in a difficult problem.

In the following chapter, we consider a case for which we know there are far reaching results. It is hoped that the insight gained will allow us to make further progress with the more realistic and difficult problems introduced in this chapter.

[9] For completeness the full bifurcation diagram should be constructed. However, for our purposes it is sufficient to consider the behaviour of the critical line $(\beta, n^*(\beta))$.

Chapter 4

The quasi-static viscous case

4.1 Introduction

In this chapter we diverge from our solution strategy to carry out an analysis of the drainage mechanism around a quasi-realistic symmetric smooth probe that is applicable to the case of a very slow moving oil droplet. This is arguably the "worst" case from the point of view of the measurement principle, since such a droplet will take the longest time to rupture. Further, we hope that the insight gained will result in a deeper understanding of the drainage mechanism for faster moving oil droplets.

Consider the static version of the two-dimensional model problem. Set $U_\infty \equiv 0$, $\theta \equiv 0$ and suppose the probe protrudes a fixed and specified displacement distance $d = O(D)$ into the oil, relative to the undisturbed interface (see figure 4.1). The configuration could be mimicked experimentally by pushing the probe into the interface sufficiently slowly. However, for large enough d the problem is certainly physically artificial.

It is clear that this removes the natural velocity scale, which must therefore be determined by a balance of the driving forces. The only dimensionless parameter independent of the velocity scale, $\overline{U}$ say, is the Bond number Bo, which is typically small (see table 2.2). Hence, typically, surface tension dominates over gravity on all arcs of the interface with typical radius of curvature, R_I say, less than or equal to the diameter D of the probe. In extreme cases the Bond number can reach order unity values, so that these forces balance on all arcs of the interface with $R_I \sim D$.

To progress further we must make some additional assumptions. Motivated by the fact that we are interested in the final stages of drainage of the water film, we assume that (i) the interface is almost at rest, so that inertia is negligible throughout, and that (ii) the film surrounding the probe tip is thin compared to its length. The first fundamental assumption guarantees that the driving forces in the thin film are viscous shear, together with surface tension or gravity, or both, depending on the size of the Bond number, and on the typical size, $1/R_p$ say, and behaviour of the substrate curvature. Assumption (ii) then allows us to apply a classical lubrication approach, and therefore decompose the liquid domain into three or more regions which may be analysed separately and either formally matched or informally patched together.

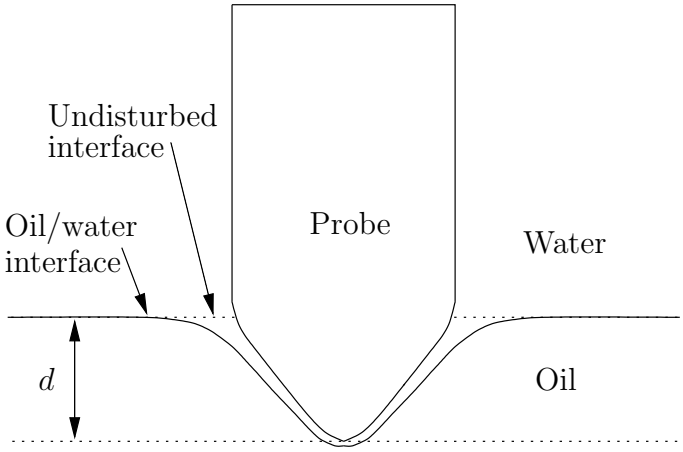


Figure 4.1: Schematic diagram of the set-up.

We concentrate on the generic case where the *rounded* probe cone consists of a *curved* substrate arc with typical radius of curvature $R_p \sim D$. This captures a wide class of plausible probe shapes.

In section 4.2 we detail the geometrical set-up and convert the dimensional governing equations into a probe-based orthogonal curvilinear coordinate system. In section 4.3, we derive the "outer" solution for the zero-thickness film dominated by capillary-statics. Then, in section 4.4 we investigate the flow of the water in the thin film on a rounded cone ($R_p \sim D$). The thin film subtends an arc length around the probe that is entirely determined by the outer problem. This aside, the inner and outer problems de-couple. In section 4.5 we discuss the "transition" region through which the inner and outer solutions are either informally "merged" or formally matched together. We consider a naïve matching strategy and use it to explain why a certain very elegant procedure is formally necessary. The physical implications are startling and suggest that a more careful asymptotic analysis is required. We discuss these and other possible extensions in section 4.6.

We emphasise that, since the dominant force balances in each of the regions is different from those presented in chapter 3, it is convenient to break away from convention and nondimensionalise the inner and outer problems as we come to them.

4.2 Governing equations in the new coordinate system

4.2.1 Geometry of the substrate

We suppose that the probe surface is given by

$$\mathbf{r_p} = \mathbf{r_p}(s) = (x_p(s), z_p(s)), \tag{4.1}$$

where s is arc length from the tip O measured in an anti-clockwise sense. The basic assumption we make is that the even functions x_p and z_p are monotonic increasing on $[0, \infty)$. We call a probe *sharp* if, in addition, $z_p(s)$ is strictly monotonic increasing on $[0, \infty)$.

We define the positively oriented unit tangent vector $\mathbf{t_p}(s)$, unit normal vector $\mathbf{n_p}(s)$ and curvature $\kappa_p(s)$ by the usual Serret-Frenet formulae:

$$\mathbf{t_p} = \tfrac{d\mathbf{r_p}}{ds}, \ \tfrac{d\mathbf{t_p}}{ds} = -\kappa_p \mathbf{n_p}, \ \tfrac{d\mathbf{n_p}}{ds} = \kappa_p \mathbf{t_p}. \tag{4.2}$$

Let $\chi_p(s)$ be the acute angle $\mathbf{t_p}(s)$ makes with the positive x-axis, then

$$\kappa_p = \tfrac{d\chi_p}{ds} \quad \text{and} \quad \mathbf{r_p}(s) = \textstyle\int_0^s (\cos\chi_p(\zeta), \sin\chi_p(\zeta))\, d\zeta. \tag{4.3}$$

For simplicity, we assume that κ_p is at least continuously differentiable and suppose that $s = \pm s_0$ corresponds to the end of the cone[1] (see figure 4.2). We define the following types of arc on the probe:

- An arc is *curved* if its curvature is not constant on any sub-arc it contains.
- An arc is *straight* if its curvature is identically zero and *circular* if its curvature is identically a non-zero constant.
- An arc is (*strictly*) *monotonic* if its curvature is an (strictly) increasing function of distance from the origin.

The majority of probes in use are sharp and have at least a monotonic probe cone.

4.2.2 The new coordinate system

We employ probe-based orthogonal curvilinear coordinates (s, n) to describe a point in the liquid domain whose position is

$$\mathbf{r}(s, n) = \mathbf{r_p}(s) + n\mathbf{n_p}(s). \tag{4.4}$$

The required vector identities are readily derived. For example, if $f(s, n)$ is a scalar field and $\mathbf{F}(s, n) = (F_1, F_2)$ is a vector field, then

$$\nabla f = \frac{1}{h_1} f_s \mathbf{t_p} + f_n \mathbf{n_p},$$

[1] This means that the probe cone joins smoothly onto the upper cylindrical body.

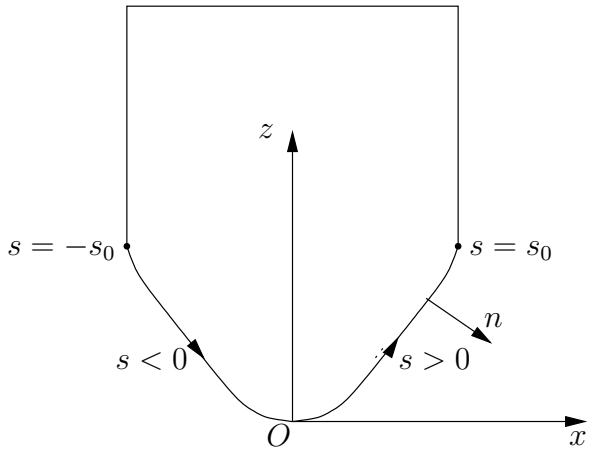


Figure 4.2: Cartesian $O(x, z)$ and orthogonal curvilinear $O(s, n)$ coordinate systems.

$$\nabla \cdot \mathbf{F} \quad = \quad \frac{1}{h_1}(F_{1s} \, + \, (h_1 F_2)_n),$$

where the metric coefficients are given by,

$$h_1 \, = \, |\frac{\partial \mathbf{r}_p}{\partial s}| \, = \, 1 \, + \, \kappa_p \, n \quad \text{and} \quad h_2 \, = \, |\frac{\partial \mathbf{r}_p}{\partial n}| \, = \, 1. \tag{4.5}$$

For clarity, the two coordinate systems we use are illustrated in figure 4.2.

4.2.3 Governing equations

In the new coordinate system, S say, the local hydrostatic pressure in each fluid is $\rho_i g Z(s, n)$, up to the addition of an arbitrary constant, where

$$Z(s, n) = n \cos \chi_p(s) - z_p(s).$$

Writing the velocity fields in the oil and water as

$$\mathbf{u_i} \quad = \quad u_i \mathbf{t_p} \, + \, w_i \mathbf{n_p},$$

the continuity equation (2.1) in the new coordinate system, reads

$$u_s + (h_1 w)_n \quad = \quad 0. \tag{4.6}$$

In (4.6) and hereafter, where the same equation applies to both fluids, we drop subscripts for ease of notation.

The first fundamental assumption (i) of section 4.1, implies that our governing momentum equations are the Stokes slow flow equations, which take the following rather cumbersome component form:

$$\begin{aligned} \frac{1}{h_1} p_s \quad = \quad & \mu \Big(\frac{1}{{h_1}^2} u_{ss} + u_{nn} - \frac{n}{{h_1}^3} (\kappa_p)_s u_s + \frac{\kappa_p}{h_1} u_n \\ & - \frac{\kappa^2}{{h_1}^2} u + \frac{1}{{h_1}^3} (\kappa_p)_s w + \frac{2\kappa_p}{{h_1}^2} w_s \Big), \end{aligned} \tag{4.7}$$

$$\begin{aligned} p_n &= \mu\Big(\frac{1}{{h_1}^2}w_{ss} + w_{nn} - \frac{n}{{h_1}^3}(\kappa_p)_s w_s + \frac{\kappa_p}{h_1}w_n \\ &\quad - \frac{\kappa^2}{{h_1}^2}w - \frac{1}{{h_1}^3}(\kappa_p)_s u - \frac{2\kappa_p}{{h_1}^2}u_s\Big). \end{aligned} \tag{4.8}$$

The no-slip boundary condition (2.3) on the probe surface simply becomes,

$$\mathbf{u_1} = \mathbf{0} \quad \text{on} \quad n = 0. \tag{4.9}$$

To find the interfacial boundary conditions relative to S, we suppose that the interface I is given by,

$$\mathbf{r_I} = \mathbf{r_I}(s_I, t) = \mathbf{r}(s, h(s,t)), \tag{4.10}$$

where $s_I = s_I(s,t)$ is the arc length along the interface, measured from the axis of symmetry in the same sense as s. Define the interface unit tangent vector $\mathbf{t_I}(s_I,t)$, unit normal vector $\mathbf{n_I}(s_I,t)$ and curvature $\kappa_I(s_I,t)$ by,

$$\mathbf{t_I} = \frac{\partial \mathbf{r_I}}{\partial s_I}, \ \frac{\partial \mathbf{t_I}}{\partial s_I} = -\kappa_I \mathbf{n_I}, \ \kappa_I = \frac{\partial \chi_I}{\partial s_I}. \tag{4.11}$$

The corresponding "tangential" angle $\chi_I(s_I)$ is the angle between $\mathbf{t_I}(s_I,t)$ and the positive x axis measured in the same sense as $\chi_p(s)$.

Using (4.2) through (4.11), we deduce the following geometric identities:

$$\begin{aligned} \frac{\partial s}{\partial s_I} &= \frac{1}{({h_1}^2 + {h_s}^2)^{\frac{1}{2}}}, \\ \frac{\partial^2 s}{\partial {s_I}^2} &= -\frac{h_1(h_1)_s + h_s h_{ss}}{({h_1}^2 + {h_s}^2)^2}, \\ \mathbf{t_I} &= \frac{h_1}{({h_1}^2 + {h_s}^2)^{\frac{1}{2}}}\mathbf{t_p} + \frac{h_s}{({h_1}^2 + {h_s}^2)^{\frac{1}{2}}}\mathbf{n_p}, \\ -\kappa_I \mathbf{n_I} &= \left(h_1\left(\frac{\partial^2 s}{\partial {s_I}^2}\right) + ((\kappa_p h)_s + \kappa_p h_s)\left(\frac{\partial s}{\partial s_I}\right)^2\right)\mathbf{t_p} \\ &\quad + \left(h_s\left(\frac{\partial^2 s}{\partial {s_I}^2}\right) + \ (h_{ss} - h_1\kappa_p)\left(\frac{\partial s}{\partial s_I}\right)^2\right)\mathbf{n_p}. \end{aligned} \tag{4.12}$$

Then, the kinematic condition (2.4) is,

$$\mathbf{u_1} = \mathbf{u_2} \quad \text{and} \quad w_I = h_t + \frac{u_1}{h_1}h_s \quad \text{on} \quad n = h. \tag{4.13}$$

The normal and tangential stress conditions given by (2.5) become,

$$\sigma\kappa_I - \Delta\rho g\, Z(s,n) = (p_1 - p_2) - \mathbf{n_I}\cdot(\mu_1\mathbf{e_1} - \mu_2\mathbf{e_2})\cdot\mathbf{n_I} \ \text{ on } n = h, \tag{4.14}$$

$$0 = \mathbf{t_I}\cdot(\mu_1\mathbf{e_1} - \mu_2\mathbf{e_2})\cdot\mathbf{n_I} \ \text{ on } n = h, \tag{4.15}$$

respectively, where, for the two-dimensional Newtonian liquids, the rate of strain tensors $\mathbf{e_i}$ with respect to S, are given by

$$\mathbf{e} = \begin{pmatrix} \frac{2}{h_1}(u_s + \kappa_p w) & \frac{1}{h_1}w_s + h_1(\frac{1}{h_1}u)_n \\ \frac{1}{h_1}w_s + h_1(\frac{1}{h_1}u)_n & 2w_n \end{pmatrix}, \tag{4.16}$$

and $\mathbf{t_I}$, $\mathbf{n_I}$, κ_I are determined by the geometrical identities (4.12).

Finally, we comment that the boundary conditions at infinity are best expressed relative to the Cartesian coordinate system:

$$\begin{aligned} \mathbf{u_1},\ \mathbf{u_2} &\sim \mathbf{0} \quad \text{as } |\mathbf{x}| \to \infty, \\ \eta(x,t) &\sim d \quad \text{as } |x| \to \infty, \end{aligned} \tag{4.17}$$

where $z = \eta(x,t)$ is the Cartesian equation of the free surface.

4.3 The outer problem

Suppose the thin film subtends an arc length L around the probe tip and is of typical thickness h_0. The second fundamental assumption (ii) of section 4.1, says that the aspect ratio $\epsilon = h_0/L$ is small, i.e. $\epsilon \ll 1$. The outer solution is simply the global leading order solution to a regular perturbation in the small parameter ϵ. Setting $\epsilon = 0$, we work on a scale in which the film thickness and fluid velocities are zero. Hence, Capillary statics dominate and the problem reduces to solving the Laplace-Young equation for the free surface $z = \eta(x)$.

Our aim is therefore to determine the location of the contact points, at $s = \pm s_c$ say, and the curvature of the interface there, $(\kappa_I)_c$ say, for subsequent matching.

We note that the interface intersects the probe surface tangentially, since a discontinuity in gradients would produce a force at the contact point that could not be supported by the fluid medium. A schematic diagram of the outer problem is shown in figure 4.3.

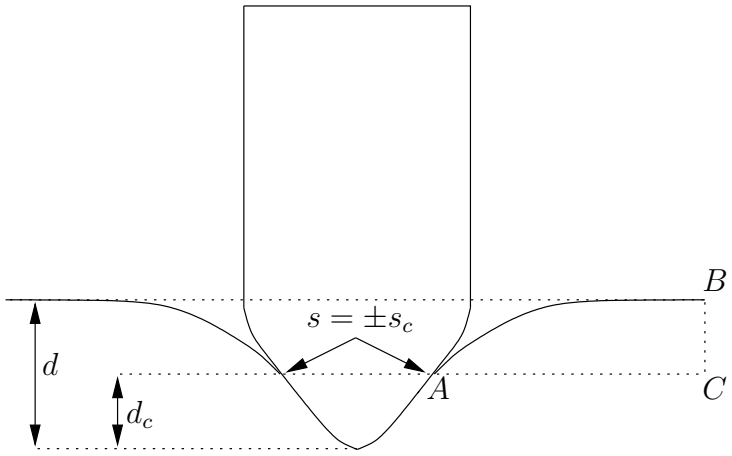


Figure 4.3: Schematic diagram of the outer problem.

4.3.1 Analytic solution

It is convenient to work in the Cartesian coordinate system. By symmetry, we consider the right-hand arc only and let the superscript "out" denote the corresponding leading

order outer variable. For example, the curvature of the interface in the leading order outer problem is $\kappa_I^{(out)}$.

The arguments presented above show that the normal stress condition reduces to the Laplace-Young equation, which balances surface tension with pressure jump across the interface, and reads

$$\sigma\kappa_I^{(out)} \quad = \quad -\Delta\rho g\eta^{(out)}. \tag{4.18}$$

Nondimensionalising $\kappa_I^{(out)}$ and $\eta^{(out)}$ with their generic values, namely $1/D$ and D, we find

$$\kappa_I^{(out)} \quad = \quad -Bo\,\eta^{(out)}, \tag{4.19}$$

where $Bo = \Delta\rho g D^2/\sigma$ is the Bond number, assumed to be $O(1)$. We discuss the case in which $Bo \leq O(\epsilon)$ as $\epsilon \to 0$ in section 4.6. The problem is best solved using a tangential angle $\chi_I^{(out)}$ and arc length $s_I^{(out)}$ formulation, for which the boundary conditions are,

$$\begin{aligned} \chi_I^{(out)} &= \chi_c \quad \text{at} \quad s_I^{(out)} = s_c, \\ \chi_I^{(out)} &\sim 0 \quad \text{as} \quad s_I^{(out)} \to \infty, \\ \eta^{(out)} &\sim d \quad \text{as} \quad s_I^{(out)} \to \infty, \end{aligned} \tag{4.20}$$

where $\chi_I^{(out)}(s_c) = \chi_p(s_c) = \chi_c > 0$ is the tangential angle of the probe and the interface at intersection, and we have used the fact that the interface lies along the probe surface over the thin film region, that is,

$$\begin{aligned} s_I^{(out)}(s) &\equiv s \qquad \text{for} \quad 0 \leq s \leq s_c, \\ \eta^{(out)}(x) &\equiv z_p(x) \quad \text{for} \quad 0 \leq x \leq x_p(s_c). \end{aligned}$$

The solution for $s_I^{(out)} \geq s_c$ is

$$\begin{aligned} \chi_I^{(out)} &= 4\tan^{-1}(d_1), \\ \eta^{(out)} &= d - \tfrac{4d_1}{\sqrt{Bo}(1+d_1^2)}, \end{aligned} \tag{4.21}$$

where

$$d_1(s_I^{(out)}) = \tan\left(\tfrac{\chi_c}{4}\right)\exp(-(s_I^{(out)} - s_c)\sqrt{Bo}). \tag{4.22}$$

The height of the point of intersection above the tip is therefore given by

$$d_c \quad = \quad d - \frac{2}{\sqrt{Bo}}\sin\left(\frac{\chi_c}{2}\right), \tag{4.23}$$

and the curvature of the interface there is

$$(\kappa_I)_c \quad = \quad -Bo\,d_c \quad = \quad 2\sqrt{Bo}\sin\left(\frac{\chi_c}{2}\right) - d\,Bo. \tag{4.24}$$

Observe that (4.23) represents a horizontal force balance on the fluid volume[2] ABC of figure 4.3, which in dimensional variables reads

$$\sigma - \sigma\cos(\chi_c) \;=\; \int_A^B P_1\,dz \;\;+\;\; \int_B^C P_2\,dz \;=\; \frac{1}{2}\Delta\rho g(d-d_c)^2.$$

For sharp probes, we find the following: On *curved* arcs of the probe with non-zero curvature, the probe geometry guarantees that if we know *one* of the triple (d_c, s_c, χ_c), then the other two are uniquely determined. In addition, it is clear that on *straight* arcs of the probe χ_p is constant, so there is a simple linear relationship between d_c and s_c along it. These results together with the nonlinear equation (4.23) relating $d_c \in (0,d)$ and $\chi_c \in (0,\pi/2)$ close the outer problem, although care must be taken to establish which type of arc the intersection point A lies on. We remark that $(\kappa_I)_c$ can never vanish so long as $Bo > 0$, which we have implicitly assumed throughout.

To clarify this general formulation we present a simple example.

4.3.2 Example: The circular cone tip

Consider a cone with a circular arc of dimensionless radius r that subtends an angle $\chi^* < \pi/2$ on each side of the tip. The probe can be sharp only if $r \le 1$ and we assume $r = O(1)$; see figure 4.4.

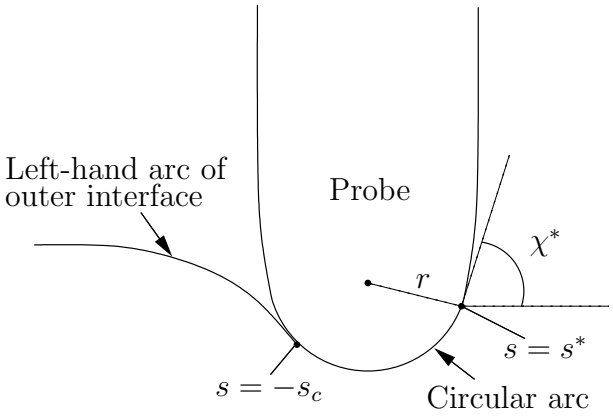


Figure 4.4: Schematic diagram of the set-up.

Suppose $\chi_c < \chi^*$, then by the geometry of the probe,

$$d_c = r(1-\cos(\chi_c)) = 2r\sin^2\left(\tfrac{\chi_c}{2}\right).$$

Hence, by (4.23), we find a quadratic equation in $\sin(\chi_c/2)$ and deduce that

$$\sin\left(\tfrac{\chi_c}{2}\right) = \frac{\sqrt{1+2rdBo}-1}{2r\sqrt{Bo}},$$

[2]This is strictly the cross-sectional area or volume per unit length in this two-dimensional problem.

which yields *the* solution if and only if $\chi_c \in (0, \chi^*)$. In this case the height and curvature at the contact point are

$$\begin{aligned} d_c &= \frac{(1+rdBo)-(1+2rdBo)^{\frac{1}{2}}}{rBo}, \\ (\kappa_I)_c &= \frac{(1+2rdBo)^{\frac{1}{2}}-(1+rdBo)}{r}. \end{aligned}$$

If $\chi_c \notin (0, \chi^*)$, the intersection point lies further up the probe and a similar analysis must be carried out there.

Observe that for Bo sufficiently small the condition $\chi_c \in (0, \chi^*)$ always holds and we have the following power series expansions valid as $Bo \to 0$:

$$\begin{aligned} \chi_c &\sim d\,Bo^{\frac{1}{2}} + O(Bo^{\frac{3}{2}}), \\ s_c &\sim rd\,Bo^{\frac{1}{2}} + O(Bo^{\frac{3}{2}}), \\ d_c &\sim rd^2 Bo + O(Bo^2), \\ (\kappa_I)_c &\sim -rd^2 Bo^2 + O(Bo^3). \end{aligned}$$

The length of the thin film L is therefore given by

$$L \sim 2rd\,Bo^{\frac{1}{2}} + O(Bo^{\frac{3}{2}}) \quad \text{as} \quad Bo \to 0. \tag{4.25}$$

■

We conclude that there is certainly an analytic solution to the outer problem for *any* sharp probe and *any* Bo > 0. In addition, we emphasize that it is essential for us to assume that the Bond number is sufficiently large that the aspect ratio of the thin film is small. By (4.25), we deduce the more general result,

$$L \sim \tfrac{2d}{\kappa_p(0)}\mathrm{Bo}^{\frac{1}{2}} \quad \text{as} \quad \mathrm{Bo} \to 0, \tag{4.26}$$

for any smooth probe tip. Hence, in dimensional variables, $\epsilon \ll 1$ if and only if the following condition holds:

$$h_0 \ll d\mathrm{Bo}^{\frac{1}{2}} \sim d\,D\,(\tfrac{\Delta\rho g}{\sigma})^{\frac{1}{2}}, \tag{4.27}$$

since $\kappa_p(0) \sim 1/D$. For simplicity, we consider the generic case in which the length of the thin film $L = O(D)$.

Finally, for subsequent matching with the flow in the thin film we detail the "outer matching condition".

4.3.3 The outer matching condition

To find the rate of divergence of the interface from a curved arc of the probe surface, we consider the configuration outlined in figure 4.5.

Here, $R_c = 1/\kappa_c$ and $(R_I)_c = -1/(\kappa_I)_c$ are the radii of curvatures of the probe surface and the interface at A, respectively, and θ is the positively oriented polar angle, with origin

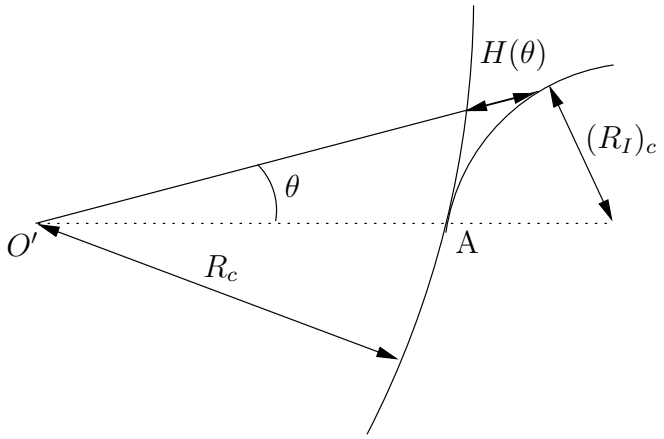


Figure 4.5: Schematic diagram of the local configuration near to A.

O' at the the centre of the circle of curvature of the probe surface at A. Finally, $H(\theta)$ is the gap between the two tangential circles of curvature through A along the ray with polar angle θ.

Elementary geometry shows that

$$H = \Big(R_c + (R_I)_c - \Big[[R_c + (R_I)_c]^2 - [R_c^2 + 2R_c(R_I)_c]\sec^2\theta\Big]^{\frac{1}{2}}\Big)\cos\theta - R_c,$$

which yields

$$H \sim \tfrac{R_c}{(R_I)_c}\Big(\tfrac{R_c+(R_I)_c}{2}\Big)\theta^2 \quad \text{as} \quad \theta \to 0.$$

Hence, as $\theta \sim (s - s_c)/R_c$ as $s \to s_c$, we deduce that

$$h^{(out)}(s) \sim \tfrac{1}{2}\kappa_{total}\,(s - s_c)^2 \quad \text{as} \quad s \to s_c, \tag{4.28}$$

where the *total* curvature of the surfaces at A is defined by $\kappa_{total} = \kappa_c - (\kappa_I)_c$. Further, if A lies on a straight arc of the probe surface where $\kappa_c \equiv 0$, the corresponding result is exactly (4.28), as expected.

We emphasize that s_c and κ_{total} are entirely determined by the outer solution for all sharp probes and any Bo > 0.

4.4 Thin film analysis

In this section we consider the thin film on the rounded cone using the probe-based coordinate system. Starting from the dimensional equations introduced in section 4.2, we establish the dominant force balances and use the resulting pressure and velocity scalings as a basis for nondimensionalisation. We then derive an evolution equation for the film height using the continuity of flux. Finally, we analyse this equation and discuss its implications with regard to the drainage delay effect.

We suppose that the thin film runs from $s = -s_1$ to s_1 around the probe tip and let $J = (-s_1, s_1)$, where $s_1 = \min(s_0, s_c)$ and we recall that $s = \pm s_0$ corresponds to the start of the upper cylindrical body.

4.4.1 Preliminaries

We begin with two results that are essential to the subsequent analysis.

The first is a power series expansion for the interfacial curvature κ_I in the small parameter ϵ. Clearly $\kappa_I \equiv \kappa_p$ on J when $\epsilon = 0$, so we nondimensionalise the curvatures κ_p and κ_I, arc length s and film height h with $1/R \sim 1/R_I \sim 1/R_p$, $D \sim L$ and $\epsilon D = h_0$ respectively. After a rather messy and tedious manipulation of the geometrical identities (4.12), we find,

$$\kappa_I \quad \sim \quad \kappa_p - \epsilon\Big(\frac{R}{D}h_{ss} + \frac{D}{R}\kappa_p^2 h\Big) + O\Big(\epsilon^2\frac{R}{D}, \epsilon^2\frac{D}{R}, \epsilon^2\Big(\frac{D}{R}\Big)^2, \epsilon^2\Big) \text{ as } \epsilon \to 0. \tag{4.29}$$

The second is the exact dimensional flux conservation equation in the orthogonal coordinate system S. Integrating the continuity equation (4.8) from $n = 0$ to $h(s,t)$ and applying (4.9) and (4.13), we find,

$$h_1(h_t + \tfrac{u_1}{h_1}h_s)|_{n=h} + \tfrac{\partial}{\partial s}\textstyle\int_0^h u_1\, dn - (u_1 h_s)|_{n=h} = 0,$$

which simplifies to give the desired equation,

$$h_1 h_t + Q_s = 0, \tag{4.30}$$

where the flux is

$$Q(s,t) = \textstyle\int_0^{h(s,t)} u_1\, dn. \tag{4.31}$$

4.4.2 Driving forces and nondimensionalisation

We consider a rounded cone on which $R_p = O(D)$. The first result of the previous section shows that curvature of the interface is, to leading order in ϵ, equal to the curvature of the substrate. Hence, if the Bond number is small, substrate induced surface tension dominates over gravity on J, while if the Bond number is order unity, these forces balance on J. Both cases are accounted for simultaneously by balancing the pressure jump with surface tension in the normal stress condition. For a non-trivial solution the pressure gradient must balance with viscous forces in the tangential momentum equation. The two dominant balances are

$$\overline{P} \sim \tfrac{\sigma}{D} \quad \text{and} \quad \tfrac{\overline{P}}{D} \sim \tfrac{\mu_1 \overline{U}}{\epsilon^2 D^2},$$

respectively, where $\overline{P}$ is the pressure scaling. Hence the velocity scale in the thin film is

$$\overline{U} \sim \tfrac{\epsilon^2 \sigma}{\mu_1},$$

and the reduced Capillary number is $Ca^* = (\mu_1 \overline{U})/\epsilon\sigma \sim \epsilon$, so that viscous stress at the free-surface is small in comparison with surface tension. We comment that the ratio of inertial to viscous forces is given by the reduced Reynolds number

$$Re^* = \epsilon^4 \tfrac{\rho_1 \sigma D}{\mu_1^2},$$

which is typically very small, as required for the lubrication theory to be valid.

This motivates the following nondimensionalisation of the field equations and the boundary conditions:

$$\begin{aligned} s &= D\,s^*, \\ n &= \epsilon D\,n^*, \\ u_\alpha &= \tfrac{\epsilon^2\sigma}{\mu_1}u_\alpha^*, \qquad (\alpha = 1,2), \\ w_\alpha &= \tfrac{\epsilon^3\sigma}{\mu_1}w_\alpha^*, \qquad (\alpha = 1,2), \\ Q &= \tfrac{\epsilon^3\sigma D}{\mu_1}Q^*, \\ p_\alpha &= \tfrac{\sigma}{D}p_\alpha^*, \qquad (\alpha = 1,2), \\ \kappa_p &= \tfrac{1}{D}\kappa_p^*, \\ \kappa_I &= \tfrac{1}{D}\kappa_I^*. \\ t &= \tfrac{\mu_1 D}{\epsilon^2\sigma}t^*, \end{aligned} \tag{4.32}$$

4.4.3 Asymptotic expansions

We hunt for solutions in the form of asymptotic expansions in powers of the small parameter ϵ:

$$u \sim u^{(0)} + \epsilon u^{(1)} + \epsilon^2 u^{(2)} + \ldots, \quad w \sim w^{(0)} + \epsilon w^{(1)} + \epsilon^2 w^{(2)} + \ldots,$$

and so on. We substitute these into (4.6) through (4.15) and equate like powers of ϵ. We show that the resulting leading-order problem is closed and therefore find it convenient to drop superscripts hereafter.

4.4.4 The leading-order problem

The Stokes equations in the water become, upon dropping stars,

$$\frac{\partial p_1}{\partial s} \sim \frac{\partial^2 u_1}{\partial n^2} + O(\epsilon), \tag{4.33}$$

$$\frac{\partial p_1}{\partial n} \sim O(\epsilon^2). \tag{4.34}$$

The fluid velocity and reduced pressure in the oil vanish in the leading order outer problem, so $|\mathbf{u_2}^{(out)}|$, $p_2^{(out)} = o(1)$ as $\epsilon \to 0$. Hence, $p_2 = 0$ to leading order in the inner thin film problem. Similarly, the drag produced by the motion of the oil, through the tangential stress condition, does not enter the leading order inner thin film problem.[3]

The normal stress condition (4.14) therefore becomes

$$p_1 \sim \kappa_I - Bo\,Z(s,0) + O(\epsilon Bo, \epsilon\frac{Ca^*}{m}) \quad \text{on} \quad n = h, \tag{4.35}$$

[3]These results are noted by Jones & Wilson [7] for a very similar problem concerning droplet coalescence.

where we recall that the viscosity ratio $m = \mu_1/\mu_2$ and the nondimensional interface curvature is given by (4.29) with $R = D$:

$$\kappa_I \quad \sim \quad \kappa_p - \epsilon\Big(h_{ss} + \kappa_p^2 h\Big) + O(\epsilon^2). \tag{4.36}$$

The tangential stress condition (4.15) becomes

$$\frac{\partial u_2}{\partial n} \quad \sim \quad O\Big(\epsilon, \epsilon\frac{1}{m}\Big) \quad \text{on} \quad n = h. \tag{4.37}$$

Since $Bo \leq O(1)$, $m = O(1)$ and $Ca^* \sim \epsilon$ as $\epsilon \to 0$, we may tidy up the errors to the leading order terms, and hereafter do so implicitly.

4.4.5 The evolution equation for the film height

From (4.34) and (4.35),

$$p_1 \quad \sim \quad \kappa_I + Bo\, z_p(s) + O(\epsilon), \tag{4.38}$$

where we have used the fact that $Z(s,0) = -z_p(s)$. Solving (4.33) for u_1, and applying the no-slip and tangential stress boundary conditions, yields

$$u_1 \quad \sim \quad \frac{1}{2}\frac{\partial p_1}{\partial s} n(n-2h) + O(\epsilon), \tag{4.39}$$

corresponding to a parabolic velocity profile in the thin film.

Since $\frac{dz_p}{ds}(s) = \sin\chi_p(s)$, the flux is

$$Q \quad \sim \quad -\frac{h^3}{3}\Big(\frac{\partial \kappa_I}{\partial s} + Bo\sin\chi_p(s)\Big) + O(\epsilon). \tag{4.40}$$

Hence, by the exact flux conservation equation (4.30) and the curvature relation (4.36), the evolution equation for the film height h is, to leading order,

$$\frac{\partial h}{\partial t} \quad = \quad \frac{\partial}{\partial s}\Big(\frac{h^3}{3} q(s)\Big) \quad \text{where} \quad q(s) := \frac{d\kappa_p}{ds}(s) + Bo\sin\chi_p(s). \tag{4.41}$$

Observe that (4.41) is also the correct asymptotic form of the evolution equation if the curvature of the arc is (i) exactly constant or (ii) constant to leading order (i.e. the arc is not curved to leading order), if and only if the Bond number is order unity. The first corresponds to a straight or circular arc, while the second corresponds to a slightly perturbed straight or circular arc; these are indistinguishable in the outer problem. The special case in which either (i) or (ii) hold and Bo $\leq O(\epsilon)$ is beyond the scope of this thesis, although we briefly discuss a method of attack in section 4.6.

4.4.6 Analysis and discussion

The evolution equation (4.41) (valid up to $O(\epsilon)$) is a first order hyperbolic partial differential equation for $h(s,t)$. It is degenerate at points s^* such that $q(s^*) = 0$. It is straightforward to show that, at a degenerate point $s^* \in J$, the solution h *either* tends to zero like $t^{-\frac{1}{2}}$ *or* blows up in finite time, depending on whether $q_s(s^*)$ is negative *or* positive, respectively.

It is clear that *all* probe shapes have a degenerate point at the origin that is well-behaved if and only if the tip is sufficiently sharp, corresponding to $q_s(0) < 0$.

Consider the class of monotonic probes. Since the curvature is not constant in this regime, the first term of q, namely $\frac{d\kappa_p}{ds}$, is monotonic decreasing on J, with a single zero at the origin. The second term, $Bo \sin\chi_p(s)$ is *strictly* monotonic increasing on J, with a single simple zero at the origin. Hence, there aremonotonic probes for which there are any given finite number of degenerate points on J, each of which can be singular. A strictly monotonic probe has a single degenerate point at the origin, unless $q_s(0) > 0 > q_s(s_1)$, in which case the there are a further two degenerate points at $s = \pm\tilde{s}$ for some $\tilde{s} \in (0, s_1)$. For a sufficiently *strong* monotonic probe corresponding to $q_s < 0$ on $[0, s_c)$, the thin film is well-behaved.

At the origin where $h_s \equiv 0$, we have $h_t = \frac{h^3}{3} q_s(0)$, which may be integrated to yield

$$h(0,t) = \frac{h(0,0)}{\sqrt{1-\frac{2}{3}q_s(0)h(0,0)^2 t}} \quad \text{with} \quad q_s(0) = \frac{d^2\kappa_p}{ds^2}(0) + Bo\,\kappa_p(0). \tag{4.42}$$

This shows that for a sufficiently sharp probe tip, corresponding to $q_s(0) < 0$, the film thins at the origin at a rate increasing with $-q_s(0)$, that is, with the "sharpness" of the probe tip. This is certainly in accordance with physical intuition. Moreover, if $q_s(0) < 0$, the rupture time t_{rup} is bounded above by the time it takes for the thin film at the origin to reach the critical rupture value. In dimensional variables this reads

$$t_{rup} \leq \frac{3\mu_1}{2\left(\sigma\frac{d^2\kappa_p}{ds^2}(0) + \Delta\rho g\kappa_p(0)\right)}\left(\frac{1}{(h_0)^2} - \frac{1}{(h_{rup})^2}\right), \tag{4.43}$$

where h_0 is the initial dimensional film thickness at the origin and h_{rup} is the dimensional rupture thickness.

To establish how close this upper bound is to the actual rupture time we consider the general solution of (4.41). This is easily found using the method of characteristics, which yields

$$h(s,t) = h_0(r)\left(\frac{q(r)}{q(s)}\right)^{\frac{1}{3}}, \tag{4.44}$$

where h_0 is the initial profile on $(-s_c, s_c)$ and the characteristic projection $s = s(r,t)$, through the point $(r,0)$ in the (s,t) plane, has speed

$$\frac{\partial s}{\partial t} = -h_0(r)^2 q(r)^{\frac{2}{3}} q(s)^{\frac{1}{3}} \quad \text{for} \quad s \neq 0, \tag{4.45}$$

and is therefore given by

$$\int_r^s \frac{1}{q(\zeta)^{\frac{1}{3}}}\, d\zeta \;+\; t(q(r)^{\frac{1}{3}} h_0(r))^2 \;=\; 0, \tag{4.46}$$

for all r,s $\neq 0$ such that the integral exists and q(r) $\neq 0$. The domain of definition is, at the very least, bounded by the characteristic projections $s = \pm s_*(t)$ through the end points

$(\pm s_c, 0)$ of the boundary curve. Further limitations on the domain of definition may result if q(s) vanishes of if the Jacobian $\partial s/\partial r$ vanishes on some curve in the (s,t) plane. We assume that q is sufficiently regular that h is well behaved on a supporting arc that encloses $(-s_c, s_c)$ (i.e. $s_* \geq s_c$) so that there is an overlap between the inner and the outer solutions.

The behaviour of the solution is highly dependent on the form of both q and h_0. However, for strong monotonic probes the analysis predicts the flow of fluid away from the tip (that is, *down* the curvature gradient), together with wave-steepening and therefore the possibility of shock formation. Further, we deduce the following two main results:

(i) For a sufficiently well-behaved initial profile $h_0(s) = h(s, 0)$, the film height can never tend to zero in finite time.

(ii) If (a) q is convex ($q_{ss} < 0$) and (b) $h_0(s)$ is smooth and monotonic increasing with distance from the tip (i.e. with $|s|$), then the same holds for all subsequent times.

The second result means that, given the hypotheses (a) and (b), if the film ruptures in the inner thin film region, then it will do so at the tip and the rupture time is exactly the bound on the right hand side of (4.43). We note that hypothesis (a) holds for a sufficiently sharp probe tip and, since we are pushing the probe into the interface (very slowly), we expect hypothesis (b) to hold in practice.

Observe that blow-up at a degenerate point and the formation of shocks (corresponding to the crossing of characteristics) are, in reality, smoothed out in a very small neighbourhood of the singular point by higher-order terms of the interfacial curvature. Now, the characteristics emanating from the subset $J \times \{0\}$ of the (s, t) plane cross if and only if $J^* = \{s \in J : q_s(s) > 0\}$ is not empty, and in this case, they do so first at time

$$t_{crit} = \min_{s \in J^*} \left(\frac{3}{2q_s(s)h_0(s)^2} \right) = \frac{3}{2q_s(s_{crit})h_0(s_{crit})^2} \quad \text{say.}$$

Hence, if $q(s_{crit}) > 0$, the break-down of the solution constitutes the formation of a shock, while if $q(s_{crit}) = 0$, so that $s = s_{crit}$ corresponds to a blowing-up degenerate point, the singularity is stronger; see Howell [6].

Clearly, a sufficient condition for the thin film to remain smooth and not develop shocks or blow-up in finite time, is that the supporting probe is strong monotonic. It is not clear whether the formation of such singularities in the solution would delay or speed up rupture. The analysis is beyond the scope of this thesis. The reader is referred to Howell [6] and Whitham [18] for a detailed account of these phenomena.

We comment that the simplest initial condition is a uniform profile (which certainly satisfies hypothesis (b)) and recalling the final comment of section 3.2.3 (due to Pearson), this should be sufficient.

For strong monotonic probe shapes, we have a solution in the thin film entirely determined from an initial condition, i.e. we don't need to match with the outer solution to close the problem. However, we carry out the analysis because it turns out that the results are very interesting and allow us to gain a much deeper understanding of the motion of the thin water film.

4.5 Transition region on a curved arc

We suppose $s_c < s_1$, so that the inner thin film solution terminates on the curved cone of the probe. So long as $-\lambda = q(s_c) > 0$ and for as long as the support of the inner thin film reaches the contact point at $s = s_c$, the fluids support a slender[4] transition region which formally matches the inner thin film solution to the outer capillary-static solution. If $\lambda \leq 0$, the method breaks down and it is not possible to match the inner and outer solutions using a slender transition region. Here, matching might be possible using a transition region with O(1) aspect ratio, although no attempt has been made by the author to seek it out. The corresponding matching from a sub-arc of constant or nearly constant curvature into the outer problem is briefly discussed in section 4.6.

The curvature of the interface diverges from the curvature of the probe so that free surface induced interfacial tension becomes a dominant force. We consider a naïve patching strategy and use it to explain why a certain very elegant procedure due to Wilson & Jones [20] is required.

We look near to s_c by setting $s = s_c + \delta(\epsilon)X$, where $\delta(\epsilon) = o(1)$ as $\epsilon \to 0$. The transition film must have the same order thickness and velocity scale as the inner thin film as $X \to -\infty$, since they are to be matched together by appealing to continuity of flux (or equivalently, continuity of film thickness). We are therefore left to determine the transition length scale $\delta(\epsilon)$ as $\epsilon \to 0$.

Writing $h(s,t) = H(X,t)$, and reintroducing the $O(\epsilon)$ free surface curvature term given by (4.29)[5], the governing equation (4.41) becomes,

$$\left[H^3(\lambda + \tfrac{\epsilon}{\delta^3} H_{XXX})\right]_X \sim O(\delta, \epsilon). \tag{4.47}$$

The exterior matching condition (4.28) becomes

$$\tfrac{\epsilon}{\delta^2} H_{XX} \sim \kappa_{total} \quad \text{as } X \to \infty, \tag{4.48}$$

while the matching condition with the inner thin film is

$$H(X,t) \sim h(s_c,t) \quad \text{as } X \to -\infty. \tag{4.49}$$

The natural scaling $\delta = \epsilon^{\frac{1}{2}}$ yields a non-trivial balance in the exterior matching condition (4.48). Tragically, the resulting leading order quasi-static evolution equation, namely

$$[H^3 H_{XXX}]_X \sim O(\epsilon^{\frac{1}{2}}), \tag{4.50}$$

is in no fit state to satisfy both boundary conditions. One might also be tempted to try the scaling $\delta = \epsilon^{\frac{1}{3}}$ to balance the first two terms in (4.47), but then one would immediately notice that this destroys the outer matching condition (4.48).

Integrating (4.47) and applying (4.49), the quasi-static governing equation takes the form,

$$\left[H^3(\lambda + \tfrac{\epsilon}{\delta^3} H_{XXX})\right] \sim \lambda H^3 + O(\delta, \epsilon). \tag{4.51}$$

[4] In the sense that its aspect ratio is $o(1)$ as $\epsilon \to 0$.

[5] It may be verified a posteriori that all other $O(\epsilon)$ terms do not enter the leading order evolution equation in the transition region.

The first term represents substrate induced surface tension and gravity, the second term represents the free surface induced surface tension and the constant term represents the pressure at (minus) "infinity" due to the "pulling" of the inner thin film. Hereafter, we refer to this as the "inner thin film force". The reason that any naïve matching strategy will fail is that these three forces do not balance throughout the transition region, so that (4.51) is not uniformly valid.

A much more subtle approach is required and is the subject of a paper by Wilson & Jones [20]. Here, they consider the entry of a falling film on a fixed vertical wall into a horizontal pool. The flow is characterised by a number of horizontal stationary ripples on the film just above the point of entry. The resulting leading order nondimensional thin film evolution equation takes the same form as (4.52), although in this problem, the first term represents gravity alone. The x coordinate (in the direction of gravity) and film thickness ϕ correspond to $O(1)$ and $O(\epsilon)$ variables in the dimensionless problem. The "matching" condition at $-\infty$ represents a uniform film thickness far up the wall and the solution must be matched into a static meniscus corresponding to quadratic growth at $+\infty$. The solution is found using the method of matched asymptotic expansions and results in a "wavy" infinite series of overlapping troughs and crests, whose horizontal length scales are asymptotically small (in ϵ). In the troughs, surface tension and the corresponding "inner" thin film force balance. In the crests, surface tension and gravity balance. The result is that, moving down the wave train in the direction of gravity, a trough is matched into the previous (or trailing) crest with a linear profile and into the subsequent (or leading) crest with a quadratic profile.

The film thickness in the n^{th} trough is of order $\epsilon^{3/10^n}$, while in the n^{th} crest it is of order $\epsilon^{-3/2\cdot 10^n}$, with respect to the $O(1)$ canonical variables x and ϕ. The conclusion is that the solution successfully explains the characteristic ripples, since these asymptotic sequences are so weak that they are essentially order unity after the first few terms.

We apply this approach to our transition region problem. Working with the canonical form of the governing equation (4.41), we find that substrate induced surface tension becomes important.

In order to apply the matching conditions it is necessary to assume that the region has an asymptotically small length scale *and* is slender, which may be verified a posteriori. The resulting leading order problems in the troughs and crests, together with their matching, are exactly the same as in the falling film problem. The first trough must be matched to the outer solution via the exterior matching condition. This results in a slightly different set of asymptotic sequences for the lengths and heights of the troughs and crests. We therefore detail the analysis of the first trough and crest.

The problem may be put into canonical form by applying the following trivial time-dependent rescaling,

$$H = h(s_c, t)\,\phi \quad \text{and} \quad X = \left(\frac{h(s_c,t)}{\lambda}\right)^{\frac{1}{3}} x, \tag{4.52}$$

which yields

$$\phi^3(1 + \tfrac{\epsilon}{\delta^3}\phi_{xxx}) = 1, \tag{4.53}$$

$$\tfrac{\epsilon}{\delta^2}\phi_{xx} \sim \Sigma \quad \text{as} \quad x \to \infty, \tag{4.54}$$

$$\phi \sim 1 \quad \text{as} \quad x \to -\infty, \tag{4.55}$$

where the time-dependent constant of integration

$$\Sigma = \frac{\kappa_{total}}{h(s_c,t)^{\frac{1}{3}}\lambda^{\frac{2}{3}}}. \tag{4.56}$$

We emphasise that in the following all other small terms may be shown to be negligible a posteriori. We start from the premise that $\delta(\epsilon) \to 0$ as $\epsilon \to 0$ in such a way that the transition region is slender. Clearly (H,X) cannot have the correct scalings for matching with the outer solution. To find them we look near to $x = 0$ by setting

$$x = a\,\zeta \quad \text{and} \quad \phi(x) = b\,T(\zeta),$$

where a and b are small parameters to be determined. Substituting into (4.54) and (4.55), we find

$$b^3T^3 + \tfrac{\epsilon b^4}{\delta^3 a^3}T^3T_{\zeta\zeta\zeta} = 1,$$
$$\tfrac{\epsilon b}{\delta^2 a^2}T_{\zeta\zeta} \sim \Sigma \quad \text{as} \quad \zeta \to \infty.$$

To obtain a non-trivial balance in *both*, we must set

$$\tfrac{\epsilon b^4}{\delta^3 a^3} = 1 \quad \text{and} \quad \tfrac{\epsilon b}{\delta^2 a^2} = 1,$$

corresponding to a balance of free surface induced surface tension, gravity and the inner thin film force. Hence $a = \epsilon^{\frac{3}{5}}/\delta$, $b = \epsilon^{\frac{1}{5}}$ and the leading order evolution equation and matching condition at $+\infty$ take the following form:

$$T^3T_{\zeta\zeta\zeta} = 1, \tag{4.57}$$
$$T_{\zeta\zeta} \sim \Sigma \quad \text{as} \quad \zeta \to \infty. \tag{4.58}$$

The condition for matching into the first crest is linear behaviour at $-\infty$,

$$T \sim -A\zeta \quad \text{as} \quad \zeta \to -\infty, \tag{4.59}$$

for some constant A to be found. The solution of (4.57), (4.58) and (4.59) is fully determined and may be found numerically. See Wilson & Jones [20] for the details, from which we deduce,

$$A \approx 1.03 \cdot \left(\frac{2^{\frac{1}{2}}}{\Sigma}\right)^{\frac{1}{5}} \approx \frac{1.10}{\Sigma^{\frac{1}{5}}} \quad \text{and} \quad T(\text{minimum}) \approx 1.14\left(\frac{\Sigma}{2^{\frac{1}{2}}}\right)^{\frac{3}{5}} \approx 0.93\Sigma^{\frac{3}{5}}.$$

This completes the analysis of the first trough.[6] In order to match the linear profile as $\zeta \to -\infty$ into the first crest, we must introduce the following scalings

$$\xi = c\zeta \quad \text{and} \quad C(\xi) = c\,T(\zeta),$$

where c is a small parameter to be found. Restoring the small term of $O(\epsilon^{\frac{3}{5}})$, the evolution equation in the first trough (4.57) becomes

$$\epsilon^{\frac{3}{5}}\tfrac{1}{c^3}C^3 + \tfrac{1}{c}C^3C_{\xi\xi\xi} = 1.$$

[6] Observe that it is not possible to match the solution in the first trough directly into the inner thin film solution (through the matching condition (4.52)). The reason is that the linear behaviour of T as $\zeta \to -\infty$ is not effected by the small term in the evolution equation (4.57), namely $\epsilon^{\frac{3}{5}}T^3$, when T is $O(\epsilon^{-\frac{1}{5}})$, corresponding to $\phi = O(1)$; see Wilson & Jones [20].

To obtain a non-trivial balance it is necessary to set,

$$\epsilon^{\frac{3}{5}}\frac{1}{c^3} = \frac{1}{c},$$

corresponding to a balance of free surface induced surface tension, gravity and substrate induced surface tension. Hence, $c = \epsilon^{\frac{3}{10}}$ and the leading order evolution equation is

$$1 + C_{\xi\xi\xi} = 0. \tag{4.60}$$

The solution is cubic with an arbitrary origin. This point is fixed and the solution is matched into the first trough by demanding

$$C = 0,\ C_\xi = -A \quad \text{at} \quad \xi = 0. \tag{4.61}$$

The quadratic matching condition with the second trough implies that C must have a double zero at some unknown value of ξ, $\xi_1 < 0$ say. This reads,

$$C = C_\xi = 0 \quad \text{at} \quad \xi = \xi_1. \tag{4.62}$$

The cubic solution of (4.60), (4.61) and (4.62) is fully determined. We repeat the analytic work of Wilson & Jones [20] to find

$$\xi_1 = -(6A)^{\frac{1}{2}} \quad \text{and} \quad C(\text{maximum}) = \left(\tfrac{32}{243}A^3\right)^{\frac{1}{2}}.$$

This completes the analysis of the first crest.[7] We comment that ξ_1 defines the origin of the next trough, $S(\zeta')$ say, whose matching condition at infinity reads $S_{\zeta'\zeta'} \sim C_{\xi\xi}(\xi_1)$ as $\zeta' \to \infty$.

We conclude that the height of the first trough and crest are $O(\epsilon^{\frac{1}{5}})$ and $O(\epsilon^{-\frac{3}{10}})$, respectively, with respect to the $O(1)$ canonical variables. If we were to continue the analysis we would find the following, with respect to the canonical variables, for all integers n:

$$\begin{aligned}
&\text{Length of the n}^{\text{th}}\text{ trough} && \sim \tfrac{1}{\delta}\epsilon^{\frac{1}{3}+\frac{8}{3\cdot 10^n}},\\
&\text{Height of the n}^{\text{th}}\text{ trough} && \sim \epsilon^{\frac{2}{10^n}},\\
&\text{Length of the n}^{\text{th}}\text{ crest} && \sim \tfrac{1}{\delta}\epsilon^{\frac{1}{3}-\frac{1}{3\cdot 10^n}},\\
&\text{Height of the n}^{\text{th}}\text{ crest} && \sim \epsilon^{-\frac{1}{10^n}}.
\end{aligned}$$

As noted by Wilson & Jones [20], these oscillations rapidly become so feeble as to be practically indistinguishable from unity. The way to formalise this observation is an idea due to Professor J.R. King of Nottingham University, namely to let the number of troughs and crests, m say, depend on ϵ in such a way that $m(\epsilon) \to \infty$ as $\epsilon \to 0$. This would spell disaster if an uncountable number of troughs and crests is formally needed to reach heights of order unity and therefore satisfy the matching condition at $-\infty$. Fortunately, this is not the case: For each $\epsilon > 0$, there exists a finite integer, $n(\epsilon)$ say, such that the n$^{\text{th}}$ trough and crest have heights of order unity with respect to the canonical variables. For, if we suppose

[7] Once again the solution cannot be matched directly into the inner thin film solution. The reason is that the height of the crest is $O(\epsilon^{-\frac{3}{10}})$ with respect to the order unity canonical variables.

that such an integer exists, then it must satisfy $\epsilon^{-\frac{1}{10^{n(\epsilon)}}} = k$ say, for some positive constant $k = O(1)$. It follows that $n(\epsilon) = N(\epsilon) + \tilde{n}(k)$ where

$$N(\epsilon) = \frac{\log(\log(\frac{1}{\epsilon}))}{\log 10} \quad \text{and} \quad \tilde{n}(k) = \frac{\log(\frac{1}{k})}{\log 10} = O(1).$$

The result also holds for trough heights with $\tilde{n}(k) = (2\log k)/\log 10$. We therefore define $n(\epsilon)$ to be the integer part of $N(\epsilon)$. The length of the transition region $\delta(\epsilon)$ is therefore given by

$$\delta(\epsilon) = O\Big(\frac{\epsilon^{\frac{1}{3}}}{\delta(\epsilon)} \sum_{i=1}^{n(\epsilon)} \Big(\epsilon^{\frac{8}{3\cdot 10^n}} + \epsilon^{-\frac{1}{3\cdot 10^n}}\Big)\Big) \quad \text{i.e.} \quad \delta(\epsilon) = O\Big(\epsilon^{\frac{1}{6}} \Big[\sum_{i=1}^{n(\epsilon)} \Big(\epsilon^{\frac{8}{3\cdot 10^n}} + \epsilon^{-\frac{1}{3\cdot 10^n}}\Big)\Big]^{\frac{1}{2}}\Big).$$

Moreover, we observe that, since

$$\epsilon^{\frac{1}{3}+\frac{8}{3\cdot 10^n}} = O(\epsilon^{\frac{1}{3}}) \quad \text{and} \quad \epsilon^{\frac{1}{3}-\frac{1}{3\cdot 10^n}} = O(\epsilon^{\frac{3}{10}})$$

for all positive integers n, the length of the transition region is bounded as follows:

$$O\Big(\sqrt{2n(\epsilon)}\epsilon^{\frac{1}{6}}\Big) < \delta(\epsilon) < O\Big(\sqrt{2n(\epsilon)}\epsilon^{\frac{3}{20}}\Big).$$

Hence, the aspect ratio of the transition region relative to the original nondimensional variables (s,h) is bounded above by

$$O\Big(\frac{\epsilon^{1-\frac{1}{10}}}{\delta(\epsilon)}\Big) \to 0 \quad \text{as} \quad \epsilon \to 0.$$

Finally, we may check that all other $O(\epsilon)$ terms do not enter the leading order evolution equations in the transition region, thus validating our initial assumptions.

We conclude that there exists a slender matching region consisting of a finite number of troughs and crests for each $\epsilon > 0$. The asymptotic structure of the solution near the first trough, relative to the order unity canonical variables, is illustrated in figure 4.6.

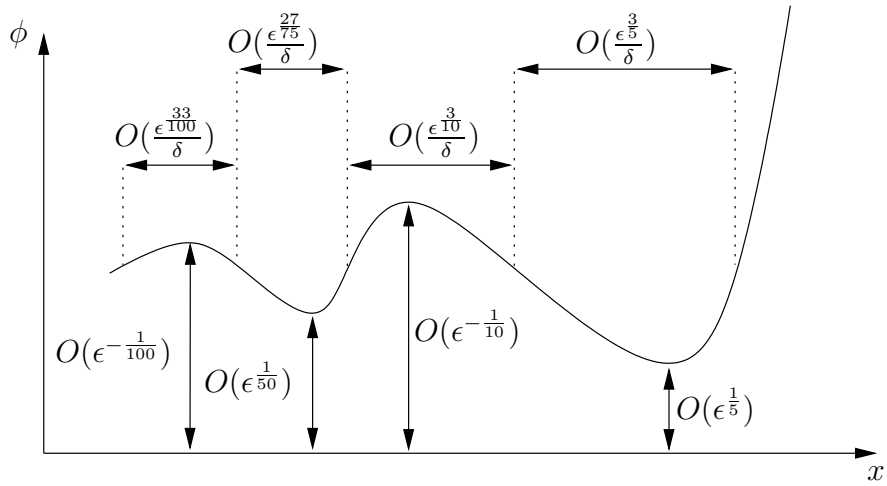


Figure 4.6: Schematic diagram of the asymptotic structure near to the first trough.

We comment that any $m(\epsilon) \geq n(\epsilon)$ will also do just as well and that this feature of the solution is a characteristic of the non-uniqueness of asymptotic expansions. We simply choose $n(\epsilon)$ as it is the minimum number necessary.

The remarkable result is that even for *extremely* small ϵ the required number of troughs and crests is small. For example,

$$\begin{array}{rcl} \epsilon \geq \exp(10^{-10}) \approx 5 \times 10^{-5} & \Rightarrow & n(\epsilon) = 1, \\ \epsilon \geq \exp(10^{-20}) \approx 5 \times 10^{-44} & \Rightarrow & n(\epsilon) = 2. \end{array} \tag{4.63}$$

The reason is clearly the presence of the $\log(\log(\cdot))$ term. In practice, we have $h_0 > h_{rup} \sim 10^{-7}$m and $L \sim D \lesssim 10^{-3}$m, so that $\epsilon \gtrsim 10^{-4}$. The implication is that in practice only a single trough and crest is needed to match the inner to the outer solution. The minimum film height in the transition region takes place in the first trough as $\epsilon \to 0$. Relative to the original nondimensional variables (s,n) it is given by,

$$h_{\min} \approx 0.93 \Sigma^{\frac{3}{5}} h(s_c, t) \epsilon^{\frac{6}{5}} \quad \text{as} \quad \epsilon \to 0. \tag{4.64}$$

The formal implication of the analysis is that the troughs are an order of magnitude thinner than the inner thin film as $\epsilon \to 0$. Hence, for sufficiently small critical rupture thickness h_{rup}, the film will always begin to rupture in the first trough. Physically, this means that a residue of water may be left behind after rupture, which could, in theory, remain in the probe measurement neighbourhood N long enough to cause gross inaccuracies in the output.

In practice there is a race between rupture in the inner thin film and in the first trough that is highly dependent on the probe geometry, the displacement distance, the initial profile of the thin film and the critical rupture thickness. We emphasize that the winner of the race can be decided quantitatively, simply by comparing the minimum film heights in the thin water film and in the first trough using typical values for the fluid properties.

4.6 Conclusions and extensions

In this chapter we diverged from our solution strategy to consider a regime for which we knew there are far reaching results, namely the quasi-static case in which the probe protrudes a fixed specified displacement distance into the oil. We carried out an analysis of the resulting drainage mechanism around a two dimensional quasi-realistic symmetric smooth probe. The analysis is applicable to the the case of a very slow far field flow and offers significant insight into the non-static case.

Our fundamental assumptions were that (i) the interface is almost at rest, so that inertia is negligible throughout, and that (ii) the film surrounding the probe tip is thin, in the sense that it has a small aspect ratio ϵ. The leading-order problem (in the small parameter ϵ) is on a scale in which the film thickness and fluid velocities are zero. Hence, Capillary statics dominate, with viscous effects negligible compared to gravity and surface tension. The relative strength of the latter two forces is given by the Bond number Bo which we assumed to be $O(1)$ throughout. The *outer* problem therefore reduces to solving the Laplace-Young equation for the free surface, with boundary conditions specified by the need for the interface to intersect the probe surface tangentially (to avoid a force singularity at the contact point) and to be flat at infinity.

We found that the resulting analytic solution had one degree of freedom, so that the outer problem was closed by appealing to the probe geometry, at least for *sharp* probes (whose coordinate in the vertical direction is a strictly monotonic increasing function of distance from the probe tip). A local analysis near to the probe tip resulted in a condition (in terms of the typical film thickness, the displacement distance, the probe curvature at the tip and the Bond number) for the thin film assumption (ii) to hold. Finally, we derived a matching condition that specified the rate of divergence of the interface from the probe surface.

Next, we considered the *inner* thin film problem. For simplicity, we concentrated on the motion of the thin water film surrounding a rounded probe cone with typical radius of curvature of the same order as the probe diameter. We showed that viscous drag becomes important and balances surface tension or gravity or both, depending on the size of the Bond number and the local probe geometry. A classical lubrication analysis resulted in a leading-order parabolic velocity profile and a thin film evolution equation, that encompasses all of the afore mentioned cases. The equation is a first-order hyperbolic partial differential equation for the film height h(s,t), which in dimensionless variables reads

$$h_t = [\tfrac{h^3}{3} q(s)]_s \quad \text{where} \quad q = \tfrac{d\kappa_p}{ds}(s) + \mathrm{Bo} \sin \chi_p(s),$$

where s is arc length along the probe surface with origin at the tip, κ_p is the probe curvature and χ_p is the tangential angle the probe makes with the horizontal. Using the method of characteristics we deduced the following main results:

- The thin film solution and its support are entirely determined by the initial film profile $h_0(s)$ and the local probe geometry via q. Further, if h_0 and q are sufficiently regular the film is well behaved and its support extends past the contact point into the outer solution. Note that we do not need to match with the outer solution to close the inner problem, which is characterised by wave-steepening and therefore the possibility of shock formation.

- A sufficient condition for the thin film to remain smooth and not develop shocks or blow-up in finite time, is that $q_s < 0$. If this holds and the initial profile is smooth, then the film height can never tend to zero in finite time. In fact, the film thickness at the origin tends to zero like $(\frac{2}{3} q_s(0) t)^{-\frac{1}{2}}$, so that the rate of thinning increases with the "sharpness" of the probe tip.

- If q is convex ($q_{ss} < 0$) and $h_0(s)$ is smooth and monotonic increasing with distance from the tip (i.e. with $|s|$), then the same holds for all subsequent times. In this case, if the film ruptures in the inner thin film region, then it will do so at the tip and the dimensional rupture time is

  $$t_{rup} = \frac{3\mu_1}{2\big(\sigma \frac{d^2\kappa_p}{ds^2}(0) + \Delta\rho g \kappa_p(0)\big)} \Big(\frac{1}{(h_0)^2} - \frac{1}{(h_{rup})^2} \Big),$$

  where μ_1 is the water viscosity, σ is the surface tension, $\Delta\rho > 0$ is the oil-water density difference, g is the acceleration due to gravity, h_0 is the initial dimensional film thickness at the origin and h_{rup} is the dimensional rupture thickness.

- Clearly, t_{rup} is a bound on the rupture time for any smooth initial profile, provided $q_s < 0$.

- Blow-up in the film height at degenerate points and the formation of shocks are, in practice, smoothed out in a very small neighbourhood of the singular point by higher-order terms of the interfacial surface tension. It is not clear whether the formation of such singularities would delay or speed up rupture.

Finally, we showed that, provided the pressure gradient in the thin film as it meets the static meniscus is negative (i.e. $q_s(s_c) < 0$), the inner thin film solution may be matched into the outer geometry using a slender transition region. The matching proved to be non-trivial, as in any problem in which a thin layer of fluid flows into a static meniscus. It was accomplished using (i) the method of matched asymptotic expansions, mirroring an elegant technique due to Wilson & Jones [20] and, (ii) an ingenious idea due to Professor J.R. King of Nottingham University. The remarkable result was that only a finite number of overlapping troughs and crests are needed to perform the matching. Indeed, in practice only a single trough and crest are need to perform the matching.

The height of the first trough is an order of magnitude smaller than in the inner thin film. Hence, for sufficiently small critical rupture thickness h_{rup}, the film will always begin to rupture in the trough. Physically, this means that a residue of water may be left behind after rupture, which could, in theory, remain in the probe measurement neighbourhood N long enough to cause gross inaccuracies in the output.

In practice, there is a race between rupture in the inner thin film and in the first trough that is highly dependent on the probe geometry, the displacement distance, the initial profile of the thin film and the critical rupture thickness. We emphasize that the winner of the race can be decided quantitatively, simply by comparing the minimum film heights in the thin water film and in the trough, using typical values for the fluid properties.

There are numerous possible extensions to the work presented in this chapter. We summarise the main ones below.

- The in-depth analysis of strong monotonic ($q_s < 0$) and other types of probe. The underlying theory may be found in Howell [6].
- Attempt to perform the transition region matching when the inner and outer regions overlap but $q_s(s_c) \leq 0$. The special case in which $q_s(s_c) \sim O(\epsilon^\alpha)$ for some $\alpha \in K \subseteq (0, \infty)$ should be amenable to the method discussed in section 4.5 for some K.
- The linear stability analysis of each of the regimes to small perturbations, both in and into the plane. The most worrying feature of the model is that we expect the outer problem to be unstable over sufficiently long time scales. Indeed, if we wait long enough we expect it to finger! All of the above analysis is therefore valid if and only if the film ruptures on an asymptotically smaller time scale, so that the instabilities do not have time to do their damage.
- The analysis of the cases in which the substrate curvature is constant to leading order on a sub-arc or on the whole probe cone *and* the Bond number is asymptotically small in the small parameter ϵ. This means that the length of the thin film around the probe tip is asymptotically small unless the displacement distance d (to which the probe penetrates past the undisturbed interface) is asymptotically large in such a way that the length of the film is order unity. In the first case, an analysis of the circular

cone tip will reveal the asymptotic structure of the inner solution for *any* smooth probe tip. The transition region will be exactly as in Jones & Wilson [7][8] resulting in an asymptotically larger thinning time scale. In the second case, the situation will be more complicated: the leading order inner thin film solution must be found on sub-arcs of the probe with curvature that is constant to leading order. These solutions must then be matched into the ajoining sub-arcs and/or the outer solution and we beleive that this may be acheived via slender transitions regions very similar to those used in section 4.5 and in Jones & Wilson [7], respectively.

- The effect of singularities (namely shocks, degenerate points that blow-up in finite time and puddles) on the the rupture time, and their interaction with the transition region. Again, the underlying theory may be found in Howell [6].

- The analysis of non-smooth probes with a corner or cusp at the tip. This will introduce delta functions and their derivatives, demanding an approach along the lines of Schwartz and Weidner [16]. Of particular interest is the inner problem in the neighbourhood of the tip.

- The generalisation of the analysis to the full three dimensional radially-symmetric problem. This will be very similar to the two-dimensional case, in each of the regions, although we note the following main differences: (i) The Laplace-Young equation must be solved numerically in the outer problem. (ii) In the inner thin film problem we expect axi-symmetric surface tension (the so-called *hoop stress*) to be significant. Indeed, for sharp probes the hoop stress will decrease with distance from the tip, but will be at least as strong as gravity on the upper cylindrical probe cone.

- The application of this decomposition to the final stages of thinning in the corresponding fully inviscid problem and finally to the full moving model problem.

In the next chapter we start work on the final extension by looking at the corresponding inner problem for the fully inviscid approximation.

[8]Their problem is that of droplet coalescence. This results in a configuration in which the probe is replaced by a rigid circular droplet that is almost at rest on the interface. It is supported by a combination of interfacial tension and buoyancy, so that the displacement distance d is implicitly specified by the resulting "outer" force balance.

Chapter 5

The inertial thinning phase

In chapter 3 we found, neglecting surface tension and the density difference, that a large number of interesting analytic solutions could be found simply by tracing streaklines in a single-phase flow. In this chapter, we reintroduce them to see whether the corresponding capillary and inertial forces can "hold-up" the interface in the neighbourhood of the probe tip where the curvature of the interface is quite high, thereby causing its rupture to take significantly longer then the time predicted by the single-phase approach. To investigate this, we consider the thin film problem that is analogous to the inner problem of the previous chapter.

5.1 Preliminaries

For simplicity, we consider exactly the same geometrical configuration as in the previous chapter, namely, a symmetric smooth probe with a cone of typical radius of curvature of the same order as the probe diameter. We employ the probe-based orthogonal curvilinear coordinate system S: (s,n).

The natural length scale over which inertia and surface tension balance is the inertial length D^I, with typical value in the range given by (2.13). On all arcs of the interface with typical radius of curvature R_I less than or equal to D^I, surface tension is significant and the non-dimensional normal stress condition (2.11) becomes,

$$p_1 = p_2 + \frac{D^I}{R_I}\kappa_I \quad \text{on} \quad I, \tag{5.1}$$

where we have rescaled κ_I with $1/R_I$ rather than $1/D$. On arcs with $R_I >> D^I$ inertia dominates over surface tension and the interface is indistinguishable from an appropriately chosen streakline. This is always the case sufficiently far from the probe, where the free-surface levels and $R_I \to \infty$.

We recall from chapter 3 that, as the interface is dragged past the probe by the far field bulk flow, it forms a film on the probe surface in some neighbourhood, M say, of the tip. Beyond a sufficiently large time, the aspect ratio ϵ of the film is small and the curvature of the interface and the probe surface are equal in M, at least to leading-order in ϵ (see

(4.29)). Hence, provided the Weber number is not too large, surface tension will certainly enter the thin film problem in M. In the large Weber number limit, the global solution is simply single-phase streakline flow. We consider the case in which the Weber number is not too large.

The outer problem is on a scale on which the film thickness is zero so the interface must meet the probe surface tangentially, at least for smooth probes. This results in a special kind of moving contact-line problem, of the type considered by Billingham & King [2] for the idealized flat plate probe. The analysis of this difficult problem is beyond the scope of this thesis. Here, we make the naïve assumption that, for sufficiently smooth probes, the problem is wellposed so that the solution determines the length of the thin film around the probe tip, from $s = -s_c(t)$ to $s_c(t)$ at time t, say. We denote the leading order pressure in the outer problem by $\mathrm{p}^{(out)}$. It is hoped that the inner and outer solutions can again be matched together by an intermediate solution, on a transition region in which the surface tension adjusts with the interfacial curvature.

In the following section, we consider the inner thin film problem in M.

5.2 The thin film problem

The dimensionless problem is detailed in chapter 2. The flow is initially irrotational, so by the classic corollary to Kelvin's Circulation Theorem, it is always irrotational and the vorticity is always identically zero, thus

$$((1 + \kappa_p n)w_i)_s - (u_i)_n = 0 \tag{5.2}$$

in the orthogonal curvilinear coordinate system $S : (s, n)$.

In the thin film we re-scale the normal components of length and velocity with the small aspect ratio ϵ. (5.2) implies that w_1 is zero, up to $O(\epsilon^2)$, so the velocity in the film is purely in the tangential direction and u_1 is independent of the normal coordinate n, at least up to this order of magnitude. Hence, expanding all dependent variables as asymptotic expansions in powers of ϵ, exactly as in section 4.4.3 for the quasi-static case, the flux (made dimensionless with $\epsilon D u_\infty$) is simply $Q \sim u_1(s,t)h(s,t) + O(\epsilon^2)$, where, here and hereafter, we drop superscripts for ease of notation. The exact flux conservation equation (4.30) becomes

$$h_t + (u_1 h)_s \sim O(\epsilon) \quad \text{in which} \quad u_1 = u_1(s,t). \tag{5.3}$$

Euler's equations for consevation of momentum become

$$\begin{aligned} u_{1t} + u_1 u_{1s} &\sim -p_s + O(\epsilon), \\ 0 &\sim -p_n + O(\epsilon). \end{aligned}$$

Hence, to leading order, the pressure is constant across the film and is given by the tangential stress boundary condition (2.11), which becomes to leading order

$$p(s,t) = \mathrm{r}p^{(out)}(s,0,t) + \tfrac{1}{\mathrm{We}}\kappa_p(s) + \tfrac{1}{\mathrm{Fr}^*}z_p(s),$$

where $p^{(out)}(s,n,t)$ is the leading order pressure in the outer problem, $\kappa_p(s)$ is the curvature of the probe surface, $z_p(s)$ is the z-coordinate of the probe surface at a distance s from the tip, and the dimensionless parameters are the density ratio r= ρ_1/ρ_2, the Weber number We= $\rho_1 U_\infty^2 D/\sigma$ and the reduced Froude number $\mathrm{Fr}^* = \rho_1 U_\infty^2/\Delta\rho g D$. They take the typical vales given in table (2.2) of section 2.3 and we therefore take them to be order unity with respect to ϵ.

The leading order thin film equations are therefore

$$h_t + (u_1 h)_s = 0, \tag{5.4}$$

$$u_{1t} + u_1 u_{1s} = -p_s, \tag{5.5}$$

where the leading order pressure gradient is given by

$$p_s(s,t) = \mathrm{r}\frac{\partial p^{(out)}}{\partial s}(s,0,t) + \frac{1}{\mathrm{We}}\frac{d\kappa_p}{ds}(s) + \frac{1}{\mathrm{Fr}^*}\sin\chi_p(s). \tag{5.6}$$

The first order hyperbolic system (5.4), (5.5) decouples: given u_1 at t=0 solve (5.5) for u_1(s,t) and then substitute it into (5.4), together with h at t=0, to find h(s,t). The equations may, in theory, be solved using the method of characteristics (c.f section 4.4.6), thus:

$$\frac{\partial u}{\partial t} = -p_s(s,t) \quad \text{and} \quad \frac{\partial h}{\partial t} = -u_{1s}(s,t)h(s,t), \tag{5.7}$$

along the characteristic projection $s = s(r,t)$ in the (s,t) plane that has speed

$$\frac{\partial s}{\partial t} = u_1(s,t) \tag{5.8}$$

and passes through the point (r,0), which, as r varies over the arc $(-s_c(0), s_c(0))$, forms the Cauchy boundary curve on which the initial data are imposed:

$$[s, u_1, h] = [r, u_1(r,0), h_0(r)] \quad \text{at} \quad t = 0. \tag{5.9}$$

The choice of a quasi-realistic initial condition for the velocity could be based on the value of the single-phase velocity on the probe surface. The film height could be taken as uniform at $t = 0$.

All of the comments concerning wellposedness of the first order hyberbolic equation (4.41) that were made in section 4.4.6 apply here with appropriate modification. The condition for a smooth solution, given smooth initial data, is that $-p_s > 0$, corresponding to a sufficiently sharp probe, in a sense which is now quantatively defined. In this case, suppose that the characteristic projections through the end points of the boundary data are $s = \pm s_*(t)$. Then, for the inner and outer solutions to overlap we require that

$$s_c(t) \le s_*(t) \quad \text{for all} \quad t \ge 0. \tag{5.10}$$

Unfortunatley, the system of characteristic equations (5.7) and (5.8) cannot, in general, be integrated to form the Riemann invariants, so there is no hope of an analytic solution of the general problem. A much deeper analysis is required to establish whether the independent condition (5.10) holds in general and, indeed, to justify the decomposition that is the backbone of our method. This said, the thin film analysis presented in this section must hold sufficiently close to the tip at sufficiently large times. We can therefore make some progress by approximating the outer pressure and considering a small s expansion in the neighbourhood of the tip.

Local solution near to the tip

The problem is symmetric about the z-axis so in the neighbourhood of the nose as s $\to$ 0 we pose the following expansions for the outer pressure, the probe geometry and the initial conditions:

$$\begin{aligned} p^{(out)}(s,0,t) &\sim -\frac{1}{2}a_0 s^2 - \frac{1}{4}a_1 s^4 + O(s^6), \\ \kappa_p(s) &\sim \kappa_p(0) - \frac{1}{2}b_0 - \frac{1}{4}b_1 s^4 + O(s^6), \\ u(s,0) &\sim c_0 s + \frac{1}{3}c_1 s^3 + O(s^5), \\ h(s,0) &\sim d_0 + d_1 s^2 + O(s^6). \end{aligned}$$

Hence by (4.3) and (5.6) the outer pressure becomes

$$p^{(out)}(s,0,t) \sim -\tfrac{1}{2}K_0 s^2 - \tfrac{1}{4}K_1 s^4 + O(s^6)$$

as $s \to 0$, where

$$\begin{aligned} K_0 &= r a_0 + \frac{b_0}{\mathrm{We}} - \frac{\kappa_p(0)}{\mathrm{Fr}^*}, \\ K_1 &= r a_1 + \frac{b_1}{\mathrm{We}} + \frac{\kappa_p(0)^3 + b_0}{6\mathrm{Fr}^*}. \end{aligned}$$

The a_i are functions of time that are assumed to be determined entirely by the leading order outer problem. Here, we argue that a useful approximation may be obtained in the neighbourhood of the nose by replacing the outer pressure by the pressure in steady single-phase oil flow around the probe and therefore take the a_i to be constant. The b_i, c_i and d_i are constants specified by the probe geometry and initial conditions near to the nose.

We comment that if the local maximum of curvature is at the tip then

$$b_0 = -\frac{d\kappa_p(0)}{ds^2} > 0,$$

and, further, that for a sufficiently sharp tip, small Weber number We and high reduced Froude number Fr* the constants K_0 and K_1 are strictly positive, which is typically the case in practice.

We seek solutions of (5.4) and (5.5) as $s \to 0$ in the form

$$\begin{aligned} u_1(s,t) &\sim u^0(t)s + u^1(t)s^3 + O(s^5), \\ h(s,t) &\sim h^0(t) + h^1(t)s^2 + O(s^4). \end{aligned}$$

Substituting and equating like powers of s the leading order problem is

$$\begin{aligned} \frac{dh^0}{dt} + u^0 h^0 &= 0, \\ \frac{du^0}{dt} + (u^0)^2 &= K_0, \end{aligned}$$

with initial conditions

$$u^0(0) = c_0 \quad \text{and} \quad h^0(0) = d_0,$$

while the first order problem is

$$\begin{aligned} \frac{dh^1}{dt} + 3u^0h^1 + 3u^1h^0 &= 0, \\ \frac{du^0}{dt} + 4u^0u^1 &= K_1, \end{aligned}$$

with initial conditions

$$u^1(0) = c_0 \quad \text{and} \quad h^1(0) = d_0.$$

The solution of the leading order problem depends crutially on whether K_0 is positive, negative or zero.

1. K_0 positive.

Suppose $K_0 = k_0^2 > 0$ for some $k_0 > 0$, say, then

$$\begin{aligned} u^0(t) &= k_0 \frac{c_0 + k_0 \tanh(k_0 t)}{k_0 + c_0 \tanh(k_0 t)}, \\ h^0(t) &= \frac{k_0 d_0}{k_0 \cosh(k_0 t) + c_0 \sinh(k_0 t)}. \end{aligned} \tag{5.11}$$

As $t \to \infty$,

$$\begin{aligned} u^0(t) &\sim k_0(1 + sgn(c_0 - k_0)e^{-2k_0 t}), \\ h^0(t) &\sim \frac{2d_0}{1 + c_0/k_0} e^{-k_0 t}, \end{aligned}$$

so the film thickness tends to zero exponentially and the outer pressure gradient and surface tension beat gravity.

2. K_0 negative.

Suppose $K_0 = -k_0^2 > 0$ for some $k_0 > 0$, say, then

$$\begin{aligned} u^0(t) &= k_0 \cot\left(\cot^{-1}(c_0/k_0) + k_0 t\right), \\ h^0(t) &= \frac{d_0}{\sin\left(\cot^{-1}(c_0/k_0) + k_0 t\right)}, \end{aligned}$$

where $\cot^{-1} : (-\infty, \infty) \to (0, \pi)$. The film thickness blows up in finite time

$$t^* = \tfrac{\pi - \cot^{-1}(c_0/k_0)}{k_0},$$

corresponding to the formation of a puddle at the tip and gravity dominating over the outer pressure gradient and surface tension.

3. K_0 zero.

Suppose $K_0 = 0$, then

$$u_0(t) = \frac{c_0}{1 + c_0 t} \quad \text{and} \quad h_0(t) = \frac{d_0}{1 + c_0 t}.$$

Here the outer pressure gradient and surface tension are exactly balanced by gravity. The behaviour of the film depends sensitively on the initial condition for the velocity $u^0(0) = c_0$:

$$\begin{aligned} c_0 < 0 \quad &\Rightarrow \quad h_0(t) \to \infty \text{ as } t \to -1/c_0, \\ c_0 = 0 \quad &\Rightarrow \quad h_0(t) \equiv d_0, \\ c_0 > 0 \quad &\Rightarrow \quad h_0(t) \to 0 \text{ as } t \to \infty, \end{aligned}$$

We conclude that we require $K_0 > 0$ for the film to thin in general. In this case it will tend to zero exponentially with decay rate equal to $\sqrt{K_0}$. An upper bound for the rupture time can be found from (5.11). To establish the shape of the film in the neighbourhood of the nose, and in particular, to see if the film thickness at the tip remains a local minimum when it starts that way, we must look at the first order problem. This is beyond the scope of this thesis.

■

5.3 Summary and extensions

The applicability of the decomposition of the flow domain into an inner and outer region that are matched together trough a transition region is not clear. Indeed, it is rather worrying that the inner and outer regions do not necessarily overlap. A deeper analysis is certainly required. Some insight into the flow dynamics might be obtained by applying a boundary integral method along the lines of Billingham & King [2]. Further, consideration of the quasi-static case, in which the outer solution is exactly the same as in the quasi-static viscous case, might give us some further insight. Indeed, if the decomposition does not work in this special case, then one would expect that it could not possibly work in the moving case.

However, the local approximate solution near to the tip discussed in section 5.2 is expected to be reasonable at large times and reveals some interesting behaviour. An analysis of the higher order terms in the coordinate expansion about the tip should reveal the behaviour of the film profile there.

Chapter 6

Conclusions and Future Work

In this final chapter we first briefly summarise the main results and discuss their implications for the industrial field. Then we highlight those extensions on which we believe further work would especially fruitfull.

6.1 Summary and discussion

This thesis was motivated by the need to model the fluid dynamics of an oil-water interface as it is advected past a small needle-like probe. Such probes are used to meter the multiphase oil-water flows that typically occur in the oil extraction industry.

In chapter 1 we detailed the physics of some measurement mechanisms employed by probes in the field. It was argued that one of the possible causes of error in the standard measurement principle is a delay in rupture due to the drainage of the thin water film that is formed between a passing oil droplet and the probe just before penetration. In order to study the significance of this so-called *drainage delay effect*, a model problem was formulated in which the base far field flow supports an infinite, initially flat interface between immiscible oil and water phases, that are advected steadily and uniformly past a semi-infinite axisymmetric probe oriented normally to the interface. The van der Waal instability model for film rupture was discussed and an empirical rupture law based on the minimal film thickness was assumed. The concept of *drainage distance* was introduced as a useful measure of the strength of the drainage delay effect.

In chapter 2 we nondimensionalised the governing equations using the typical range of values that occur in the field. Using dimensionless parameter groups we examined the relative sizes of the four forces acting: inertia, gravity, viscosity and surface tension. We found that the bulk flow is driven by inertia and, in some extremes, surface tension while the viscous effects are initially confined to thin boundary layers on the probe and the interface. The flow in the thin water film was found to be dominated by surface tension, and gravity was found to be negligible throughout.

In chapter 3 we considered the natural asymptotic regimes and approximations that decompose the two dimensional model problem. The time evolution was characterised by

the relative size of the distance of the interface from the probe tip and the thickness of the boundary layer on the probe. In the final stages before rupture, it was shown that the fluid flow in the thin water film passes through a series of *thinning* regimes in which inertial forces are gradually overtaken by viscous forces. For each of these regimes, and for those concerning the earlier stages of approach, possible solution strategies were discussed and relevant literature reviewed. The result was a framework of problems to be analysed in turn, so as to build up a comprehensive picture of the significant factors that influence the drainage delay effect. Finally, we considered the most simple set of relevant models, namely single-phase flow past the probe in which surface tension and gravity are ignored. The interface is indistinguishable from an appropriately chosen streakline and it was found that a large number of interesting and useful analytic solutions could be found simply by tracing their motion. In particular, we showed the following:

- Smooth probe shapes have streaklines that do not reach the probe in finite time. The minimum distance from the probe tip to the interface is, in general, some exponentially decaying function of time whose rate increases with the flow velocity at infinity.
- In fully inviscid symmetric flow past a probe with an acute-angled corner or cusp at the tip, any approaching streakline that initially crosses the axis of symmetry will hit the vertex in finite (algebraic) time and be instantaneously penetrated by it. The streakline will then climb up the probe.
- In fully viscous symmetric flow past an acute-angled wedge, any approaching streakline that initially crosses the axis of symmetry will hit the vertex in finite (algebraic) time only if the apex angle is less than about 102.5°. In this case, the wedge does not penetrate the streakline and the result is a pinned contact line.

It became clear that even the simplest thinning regime results in a difficult problem. We therefore decided to diverge from our solution strategy to consider a regime for which we know there are far reaching results, namely the quasi-static case in which the probe protrudes a fixed specified *displacement* distance into the oil. In chapter 4 we carried out an analysis of the resulting drainage mechanism around a two dimensional quasi-realistic symmetric smooth probe. The analysis is applicable to the the case of a very slow far field flow and offered significant insight into the non-static case.

We assumed that the interface is almost at rest, so that inertia is negligible throughout, and that the film surrounding the probe tip is thin, in the sense that it has a small aspect ratio. The leading-order solution is Capillary static, with viscous effects negligible compared to gravity and surface tension. A full analytic solution is possible, at least for sufficiently sharp probes, and a local analysis near to the probe tip resulted in a condition for the thin film assumption to hold. We concentrated on the motion of the thin water film surrounding a rounded probe cone, with typical radius of curvature of the same order as the probe diameter. We showed that viscous drag becomes important, and balances surface tension or gravity, or both, depending on their relative size and the local probe geometry. A classical lubrication analysis resulted in a leading-order parabolic velocity profile and a thin film evolution equation, that encompasses all of the afore mentioned cases. The equation is a first-order hyperbolic partial differential equation for the film height. It was solved using the method of characteristics, through which we deduced the following main conclusions:

- The solution in the thin film is entirely determined from the initial film profile on an arc around the probe tip that is entirely determined by the outer problem. Further, we do not need to match with the outer solution to close the inner problem, which is characterized by wave-steepening and therefore the possibility of shock formation.
- A necessary and sufficient condition for the thin film to remain smooth and not develop shocks or blow-up in finite time, is that the supporting probe is sufficiently sharp.
- A bound on the rupture time may be deduced by consideration of the thin film at the origin. It clearly shows that rupture is faster the sharper the probe tip.

Provided the pressure gradient is negative at the contact point, the inner thin film solution may be matched into the outer geometry using a slender transition region. The matching proved to be non-trivial, as in any problem where a thin layer of fluid flows into a static meniscus. However, it was accomplished using the method of matched asymptotic expansions, following Wilson & Jones [20], and an ingenious idea due to Professor J.R. King of Nottingham University. The remarkable result was that in practice only a single overlapping trough and crest is needed. The height of the first trough is an order of magnitude smaller than in the inner thin film. Hence, for sufficiently small critical rupture thickness, the film will always begin to rupture in the transition region. Physically, this means that a residue of water may be left behind after rupture, which could, in theory, remain in the probe measurement neighbourhood long enough to cause gross inaccuracies in the output. In practice, there is a race between rupture in the inner thin film and in the trough that is highly dependent on the probe geometry, the displacement distance, the initial profile of the thin film and the critical rupture thickness. We emphasize that the winner of the race can be decided quantitatively, simply by comparing the minimum film heights in the thin water film and in the trough, using typical values for the fluid properties.

In chapter 5 we considered the motion of the thin water film in the fully inviscid approximation with surface tension and a density contrast between the fluids. For simplicity, we focused on the case of a two dimensional quasi-realistic symmetric smooth probe, with a cone of typical radius of curvature of the same order as the probe diameter. The resulting leading order extensional thin film flow was found to be governed by a hyperbolic system of evolution equations for the film thickness and tangential velocity. Although the system decouples, it cannot, in general, be integrated to form the Riemann invariants so further analytic progress with the general case was found to be difficult. We therefore reverted to asymptotic methods and considered a coordinate expansion in the neighbourhood of the tip in which the leading order pressure in the outer problem was approximated by the corresponding single-phase pressure, which, it was argued, is reasonable at sufficiantly large times. The behaviour of the resulting leading order problem was highly sensitive to the leading order pressure gradient at the tip, and predicted that, for typical values, the film thickness tends to zero exponentially with decay rate proportional to the squareroot of minus this gradient.

6.2 Future work

The numerous possible extensions to this thesis were discussed throughout and demonstrate that a formidable amount of work remains to be done. In particular, section 3.2 discussed in detail possible methods of attack and relevant literature for some of the asymptotic regimes and approximations that may be used to decompose the drainage problem into more manageable sub-problems. Then, in section 4.6 we presented a comprehensive list of extensions relevant to the quasi-static drainage problem. Finally, in section 5.3 extensions to the fully inviscid approximation were discussed.

We finish by highlighting those extensions on which we believe further work would be especially fruitful:

- For the quasi-static viscous case the analysis of the cases in which the substrate curvature is constant to leading order on a sub-arc or on the whole probe cone *and* the Bond number is asymptotically small in the small parameter ϵ.
- The quasi-static inviscid case motivated by mathematical entertainment and by the fact that if the decomposition fails here then one would certainly expect it to fail in the moving case.
- It is thought that in practice the wetability of the probe surface to the oil and water phases severely affects the efficiency of the probe. This could be investigated by modelling the effect of introducing a very thin layer of oil on the probe surface.
- The analysis of thinning regime (ii) introduced in section 3.2.3 in which the boundary layers on the probe surface and on the near side of the interface have merged and the flow in the film is driven by both inertial and viscous forces. One might begin with a coordinate expansion of Prandtl's boundary layer equations in the neighbourhood of the tip.

Bibliography

[1] G.K. Batchelor, 1967 *Introduction to fluid dynamics*. CUP.

[2] J. Billingham & A.C. King, 1995 *The interaction of a moving fluid/fluid interface with a flat plate*. J. Fluid Mech., **296**, 325-351.

[3] F. Chorlton & M.E. O'Neil, 1989 *Viscous and compressible fluid dynamics*. Wiley.

[4] I. Eames, S.E. Belcher & J.C.R. Hunt, 1994 *Drift, partial drift and Darwin's proposition*. J. Fluid Mech., **275**, 201-223.

[5] P.D. Howell, 1998 *The draining of a two-dimensional bubble*. J. Engrg. Maths., to appear.

[6] P.D. Howell, 1998 *Surface-tension-driven flow on a moving curved surface*. J. Fluid Mech., submitted.

[7] A.F. Jones & S.D.R. Wilson, 1978 *The film drainage problem in droplet coalescence*. J. Fluid Mech., **87**, 263-288.

[8] S. Kaplun, 1954 *The role of coordinate systems in boundary-layer theory*. J. Applied Mathematics & Physics, **V**,18-41.

[9] T.G. Myers, 1998 *Thin films with high surface tension*. SIAM Review, **40**(3), 441-462.

[10] H. Ockendon & J.R. Ockendon, 1995 *Viscous flow*. Cambridge University Press.

[11] J.R.A. Pearson, 1995 *Modelling the 3-phase contact lines that move in high Reynolds number flows*. Bulletin to the Institute of Mathematics and its applications, **31**, No. 11-12, 325-351.

[12] J.R.A. Pearson, 1998 *Mechanics of a rising (oil) drop*. Schlumberger Cambridge Research internal correspondence.

[13] J.R.A. Pearson, 1998 *Mechanics of the thinning of a liquid layer on a probe surface*. Schlumberger Cambridge Research internal correspondence.

[14] J.R.A. Pearson, 1998 *Suggested flow problems: Thinning of the liquid layer over a probe in two-phase flow*. Schlumberger Cambridge Research internal correspondence.

[15] L. Rosenhead,1963 *Laminar boundary layers*. Oxford University Press.

[16] L.W. Schwartz & D.E. Weidner, 1993 *Modelling of coating flows on curved surfaces.* J. Engrg. Math., **29**, 91-103.

[17] M. Van Dyke, 1975 *Perturbation methods in fluid mechanics.* Parabolic Press.

[18] G.B. Whitham, 1974 *Linear and nonlinear waves.* Wiley.

[19] S.D.R. Wilson, 1982 *The drag-out problem in film coating theory.* J. Engrg. Math., **16**, 209-221.

[20] S.D.R. Wilson & A.F. Jones, 1983 *The entry of a falling film into a pool and the air-entrainment problem.* J. Fluid Mech., **128**, 219-230.